TITLE:

An approximate stochastic optimal control framework to simulate nonlinear neuro-musculoskeletal models in the presence of noise

Authors and affiliations:

Tom Van Wouwe[1], Lena H. Ting[2,3], Friedl De Groote[1]

[1]Department of Movement Sciences, KU Leuven, Leuven, Belgium

[2]W.H. Coulter Department of Biomedical Engineering, Emory University and Georgia Institute of Technology, Atlanta, GA, USA

[3]Department of Rehabilitation Medicine, Division of Physical Therapy, Emory University, Atlanta, GA, USA

Corresponding author:

Tom Van Wouwe.

E-mail: tom.vanwouwe@kuleuven.be.

Address: Tervuursevest 101 - bus 1501, 3001 Leuven

Abstract:

Optimal control simulations have shown that both musculoskeletal dynamics and physiological noise are important determinants of movement. However, due to the limited efficiency of available computational tools, deterministic simulations of movement focus on accurately modelling the musculoskeletal system while neglecting physiological noise, and stochastic simulations account for noise while simplifying the dynamics. We took advantage of recent approaches where stochastic optimal control problems are approximated using deterministic optimal control problems, which can be solved efficiently using direct collocation. We were thus able to extend predictions of stochastic optimal control as a theory of motor coordination to include muscle coordination and movement patterns emerging from non-linear musculoskeletal dynamics. In stochastic optimal control simulations of human standing balance, we demonstrated that the inclusion of muscle dynamics can predict muscle co-contraction as minimal effort strategy that complements sensorimotor feedback control in the presence of sensory noise. In simulations of reaching, we demonstrated that nonlinear multi-segment musculoskeletal dynamics enables complex perturbed and unperturbed reach trajectories under a variety of task conditions to be predicted. In both behaviors, we demonstrated how interactions between task constraint, sensory noise, and the intrinsic properties of muscle influence optimal muscle coordination patterns, including muscle co-contraction, and the resulting movement trajectories. Our approach enables a true minimum effort solution to be identified as task constraints, such as movement accuracy, can be explicitly imposed, rather than being approximated using penalty terms in the cost function. Our approximate stochastic optimal control framework predicts complex features, not captured by previous simulation approaches, providing a generalizable and valuable tool to study how musculoskeletal dynamics and physiological noise may alter neural control of movement in both healthy and pathological movements.

Introduction

Predictive simulations are powerful tools to study neuromechanics of movement [1], [2]. Such simulations are typically based on optimal control as a theory of motor coordination to solve the redundancy problem [3]. Current approaches focus either on detailed representations of musculoskeletal dynamics while neglecting physiological noise [2], [4], [5] or on simulating the effects of physiological noise while simplifying musculoskeletal dynamics [6]–[8]. On the one hand, deterministic simulations based on complex models have advanced our understanding of how musculoskeletal dynamics shapes movement. On the other hand, stochastic simulations based on simple models have shown that noise shapes movement kinematics and variability as well as underlying control mechanisms, including modulation of feedback. Accounting for the interaction between musculoskeletal dynamics and physiological noise might therefore be important to predict physiologically-realistic control strategies and movements. However, limited efficiency of available computational tools to simulate motor behavior in the presence of noise has hampered the use of more accurate models of musculoskeletal dynamics in stochastic simulations of movement [9]. Here, we present and test a generalizable computational framework to simulate the effect of sensorimotor noise on motor control and movement in nonlinear musculoskeletal systems.

Accounting for sensorimotor noise in movement simulations is crucial to capture movement variability and sensorimotor feedback modulation. In 1998, Harris and Wolpert minimized endpoint variability in the presence of signal-dependent motor noise to simulate open-loop controlled reaching and saccadic eye movements [10]. Including signal-dependent motor noise led to physiologically realistic bell-shaped velocity profiles and the experimentally observed trade-off between reaching time and reaching accuracy, i.e., Fitt's law. Although Harris and Wolpert clearly demonstrated the importance of accounting for noise, their stochastic simulations did not include feedback control. In general, feedback control improves performance over open-loop control in the presence of sensorimotor noise [11]. Therefore, Todorov and Jordan introduced feedback control in stochastic simulations of movement and tested optimal feedback control (OFC) as a theory of motor coordination [3], [12]. The most important prediction of optimal feedback control is arguably the minimum intervention principle: "deviations from the average trajectory are only corrected when they interfere with the task goal" [12]. Optimal feedback control has since explained many kinematic and control features of reaching and standing balance [13]–[16]. However, these studies mostly used linearized models that do not account for critical nonlinearities in movement. Further, most approaches for stochastic optimal control require the control law to be time-varying, require a quadratic cost function, and require specifying movement accuracy by a penalty term in the cost function [17], [18]. As a result, the weights in the cost function need to be hand-tuned to achieve realistic results and an obligatory tradeoff between accuracy and effort that may not necessarily be physiological emerges.

Recent computational advances have drastically improved the efficiency of deterministic movement simulations enabling the use of complex and nonlinear musculoskeletal models [2], [19] but have not been leveraged to stochastic movement simulations. In deterministic simulations, optimal control can be described by open-loop control trajectories. Therefore, these simulations can be formulated as trajectory optimization problems [20]. The introduction of direct collocation approaches to solve trajectory optimization problems improved computational efficiency compared to shooting methods by decreasing the sensitivity of the optimization objective to the decision variables [5]. Simulations based on complex models have long been solved using shooting methods that have poor convergence and long computation times when the dynamics are stiff, as in many biological movements, due to the use of

time-marching integration. In contrast to direct shooting, direct collocation eliminates the need for time-marching integration by adding the parameterized states to the decision variables and by adding the discretized dynamic equations as constraints to the optimization [21]. Computational efficiency has further been improved by implicit formulations of the system dynamics to improve the numerical condition of the optimization problem [22] and the use of automatic differentiation to compute derivative information needed by gradient-based solvers [19]. These methodological advances have enabled rapid predictive simulations based on complex musculoskeletal models [2], [4], which have been applied to test optimality principles underlying human movement [23] and to study the effect of changes in the musculoskeletal system on movement [4], [24]. However, we still lack methods to take advantage of these computational tools in stochastic simulations of movement that take into account sensorimotor noise.

Here, we apply an approach to reformulate stochastic simulations as approximate deterministic simulations, originally developed for control applications in robotics and engineering [25], to neuro-musculoskeletal simulations of movement to leverage computational advances that have been successful in improving the efficiency of deterministic simulations. The resulting framework is applicable to a broad range of movements, described by nonlinear dynamics, corrupted by additive and/or signal-dependent Gaussian noise, and controlled by time-varying feedback laws with any temporal and structural design. The method, developed by Houska et al. [26]–[29], relies on a transformation of the stochastic optimal control problem into an approximate augmented deterministic optimal control problem by approximating the generally non-Gaussian state trajectory distribution by a Gaussian state trajectory that can be described by the mean state trajectory and the state covariance trajectory. The propagation of the covariance matrix is described by Lyaponuv differential equations, which assume local invariance of the system dynamics around the mean trajectory similar to the Extended Kalman Filter [30]. The main advantage of this approach is that the resulting approximate deterministic optimal control problem can be solved with direct collocation.

We first show how our stochastic optimal control framework enables the prediction of interactions between muscle co-contraction and sensorimotor feedback, using human standing balance control as an example. While OFC has been used to predict sensorimotor feedback control of balance, individual muscles and muscle dynamics have not been modeled and it is therefore unclear whether OFC also predicts muscle co-contraction as a complementary feedforward control strategy. Specifically, OFC simulations based on joint torque-driven mechanical models capture modulation of feedback control with changes in sensory acuity [13], [31], i.e. sensory reweighting, yet it is likely that modeling activation-dependent mechanical properties of muscles will affect these predictions [32]–[34]. We simulated perturbed (platform rotations and translations) standing balance based on a multi-sensory, muscle-driven model with both feedforward and feedback control in the presence of sensory and motor noise. We demonstrate that our stochastic optimal control framework predicts contributions of both feedforward, i.e. muscle co-contraction, and feedback control during standing balance that depend on movement task, sensory acuity and muscle properties.

We next demonstrate that the stochastic optimal control framework can predict perturbed reach trajectories when nonlinear musculoskeletal dynamics are considered. Prior OFC simulations based on a point-mass model capture changes in nominal reach trajectories and feedback control depending on target shape and the presence of obstacles (i.e. task goal) [8]. However, perturbed reach trajectories deviated considerably from experimental observations, and may require more accurate representations of nonlinear multi-joint and muscle mechanics. Here, we demonstrate that our stochastic optimal control framework using a muscle-driven arm model results in improved predictions of reach kinematics in

perturbed conditions as well as detailed predictions of sensorimotor feedback and muscle level control when target shape and stability of the environment (i.e. divergent force-field) are altered [35], [36]. In addition, our model predicted muscle activity in response to perturbations, which was not possible with previous simulation models, in agreement with experimental data [8].

RESULTS

Approximate stochastic optimal control framework

We simulated movement trajectories and movement variability based on nonlinear musculoskeletal dynamics driven by optimal feedforward and feedback control policies in the presence of sensory and motor noise. For each specified task, optimal control policies were computed by minimizing the expected effort in the presence of noise. Effort was defined as the time integral of the sum of muscle excitations squared [37], leading to the following general stochastic optimal control problem:

$$\min_{\boldsymbol{e_{ff}}(t),\boldsymbol{K}(t)} : \quad J = E[\int \boldsymbol{e}^T(t)\boldsymbol{e}(t)dt]$$

$$\text{subject to: } \dot{\boldsymbol{x}}(t) = \boldsymbol{f}(\boldsymbol{x}(t), \boldsymbol{e}(t), \boldsymbol{w}_m),$$

$$\boldsymbol{g}\big(\boldsymbol{x}(t), \boldsymbol{e}(t)\big) \geq 0$$

$$\boldsymbol{e}(t) = \boldsymbol{e_{ff}}(t) + \boldsymbol{K}(t) \cdot \boldsymbol{y}_{fb}(\boldsymbol{x}(t), \boldsymbol{w}_s)$$

with $E[]$ the expected value function, $\boldsymbol{x}(t)$ the stochastic state trajectory, including joint kinematics and muscle activations, $\boldsymbol{e}(t)$ the stochastic muscle excitation trajectories, $\boldsymbol{w}_m$ a set of zero-mean Gaussian motor noise sources. The musculoskeletal dynamics $\boldsymbol{f}(\boldsymbol{x}(t), \boldsymbol{e}(t), \boldsymbol{w}_m)$ were stochastic and nonlinear. To specify different task goals, we imposed task-dependent path constraints and bounds $\boldsymbol{g}\big(\boldsymbol{x}(t), \boldsymbol{e}(t)\big)$. Muscle excitations $\boldsymbol{e}(t)$ consisted of time varying deterministic feedforward muscle excitations, $\boldsymbol{e_{ff}}(t)$, as well as feedback muscle excitations derived from a linear feedback law with deterministic time-varying feedback gains $\boldsymbol{K}(t)$ and task-dependent feedback error signals $\boldsymbol{y}_{fb}(\boldsymbol{x}(t), \boldsymbol{w}_s)$. Zero-mean Gaussian sensory noise $\boldsymbol{w}_s$ was added to the feedback error signal $\boldsymbol{y}_{fb}$. These stochastic optimal control problems were approximated by deterministic optimal control problems and then solved using direct collocation (for details, see Methods). The deterministic approximation was based on the assumption that the stochastic state trajectories could be modelled by a Gaussian distribution and could thus be described by their expected value (mean trajectory) and variance (state covariance matrix).

Contributions of muscle co-contraction and feedback control in perturbed standing balance depend on movement task, sensory acuity and muscle properties

We first demonstrate that stochastic optimal control can simultaneously predict muscle co-contraction and sensorimotor feedback contributions to motor coordination, using perturbed standing balance as an example. Although OFC can capture experimentally-identified modulations of feedback contributions that depend on sensory acuity and perturbation type [13], [38]–[40], it is unclear whether OFC predicts experimentally-observed muscle co-contraction complementing feedback during perturbed standing balance. To address limitations of prior models, we simulated standing balance using an inverted pendulum model of the body that was driven by a pair of antagonistic ankle muscles that have activation-dependent impedance (Figure 1 - A). We further investigated how the predicted muscle co-contraction depends on the model of muscle mechanical impedance, performing simulations using both a Hill-type

muscle model that accounts for the force-length and force-velocity properties of muscles [5], and an augmented Hill-type muscle that also accounts for muscle short-range stiffness that was proportional to muscle activation [32], [41]. To model background muscle activity during quiet standing, feedforward muscle activations were modeled as constants. As in prior studies using torque-driven models of perturbed standing balance [14], [31], [42], feedback contributions were modelled as a linear combination of delayed proprioceptive and vestibular cues, which encode the angle and angular velocity between the body and the platform, and gravity, respectively (Figure 1 - A). Gaussian sensory and motor noise was additive to feedback signals and muscle excitations respectively. In accordance with the literature, vestibular inputs were more noisy than proprioceptive inputs [43]. We specified the task of upright standing by imposing a constant mean upright posture and a postural sway within limits of stability. To elicit a range of feedforward and feedback control policies, we simulated both random sagittal platform rotation (Figure 1 - A) and translation (Figure 1 - B) perturbations of different magnitudes. Comparing solutions for platform rotations and translations allows sensory feedback and muscle co-contraction contributions to balance control to be differentiated as rotation and translation perturbations require different ankle muscle coordination to maintain equilibrium [44] (Figure 1 – A & B).

For platform rotations, stochastic optimal control predicted differences in postural sway and sensory reweighting as previously observed in experiments with healthy individuals and vestibular loss subjects (Figure 1– A – simulations & experiments) [31], [45], [46]. In agreement with experimental findings by Peterka for healthy adults [31] (Figure 1– A – experiments, healthy) and prior OFC results, body sway in our simulations increased quasi linearly with increasing amplitude of platform rotations and saturated at larger amplitudes where the body moved in anti-phase with the platform [47] (Figure 1– A – simulations, healthy). The simulations predicted sensory reweighting similar to that observed experimentally [14], [31], [45], [48] (Figure 1– A – experiments, healthy), with increased reliance on vestibular feedback at higher rotation magnitudes (Figure 1– A – simulations, healthy). Because proprioceptive information was modelled to be more accurate than vestibular information [43], there was a higher reliance on proprioception and the body moved in-phase with the platform at low rotation magnitudes. When removing vestibular sensory information to simulate vestibular loss subjects, the simulation predicted a quasi linear increase in sway with platform rotation amplitude (Figure 1– A – simulations, vestibular loss) consistent with experimental observations [47] (Figure 1– A – experiments, vestibular loss). In contrast to sway for healthy subjects, sway for vestibular loss subjects was predicted to follow the platform motion, as proprioception is the only source of sensory information [49]. The model predicted higher total effort in vestibular loss subjects compared to healthy subjects (not shown in figure) and loss of balance when simulated sway amplitudes became unrealistic (RMS sway values larger than 5°).

During platform rotations, moderate levels of co-contraction were predicted for vestibular loss subjects [50], but not for healthy controls (Figure 1– A – simulations, CCI in healthy-SRS and VL-SRS). In rotations, increased joint impedance due to co-contraction opposes the anti-phase movement of the ankle joint that is optimal for upright balance with minimal effort. However, co-contraction contributes to the strategy of maintaining a constant joint angle with respect to the platform, the strategy predicted when the reference to gravity is absent, as in vestibular loss subjects [31], [45], [51]. Our simulations predicted co-contraction to increase above a certain perturbation magnitude in the absence of vestibular sensory information (Figure 1– A – simulations, CCI in VL-SRS). Since all simulated strategies minimize effort, our simulations predict muscles co-contraction to reduce effort with respect to using feedback only at high perturbation magnitudes in vestibular loss subjects. However, as feedback control also increases in the absence of vestibular information, the proportion of effort due to feedback control is nevertheless higher in vestibular loss than in healthy subjects (Figure 1– A – simulations, effort in VL-SRS).

In contrast to rotations, stochastic optimal control in platform translations predicted similar increases in postural sway with increasing perturbation magnitude in healthy and vestibular loss simulations, also found experimentally [52] (Figure 1 – B - simulations). As perturbation magnitude increased, the proportion of proprioceptive feedback used in balance control decreased, but in contrast to rotations, shifted toward an equal contribution of proprioceptive and vestibular feedback. As, in translations¸ both sensory signals encode the same information but with different uncertainty levels, this shift may be understood as the sensory uncertainty becoming increasingly negligible compared to the larger expected position and velocity deviations from vertical as perturbation magnitude increases. To minimize expected effort it is therefore optimal to extract feedback information from the two modalities more and more equally as the contribution of sensory noise becomes more and more negligible compared to the kinematic deviations.

In contrast to rotations, and consistent with experimental findings [53], much larger contributions of muscle co-contraction were predicted with increasing translation perturbation magnitude in both healthy and vestibular loss subjects (Figure 1– A vs B – simulations, CCI). In translations, increased joint impedance due to co-contraction reduced body sway, which in turn reduced the relative effort of feedback corrections as perturbation magnitude increased (Figure 1–B – simulations, effort).

Taken together, stochastic optimal control predicted muscle co-contraction as a complementary strategy to sensorimotor feedback depending on the mechanical properties of the muscle, perturbation type and magnitude, and sensory acuity. Muscle co-contraction was only predicted in the simulations where the Hill-type muscle model was augmented with short-range-stiffness [32]. Although some amount of muscle co-contraction was predicted in both rotation and translation perturbations, muscle co-contraction only considerably decreased the proportion of muscle effort due to feedback control in high-amplitude translation perturbations, where muscle co-contraction helps to maintain upright posture.

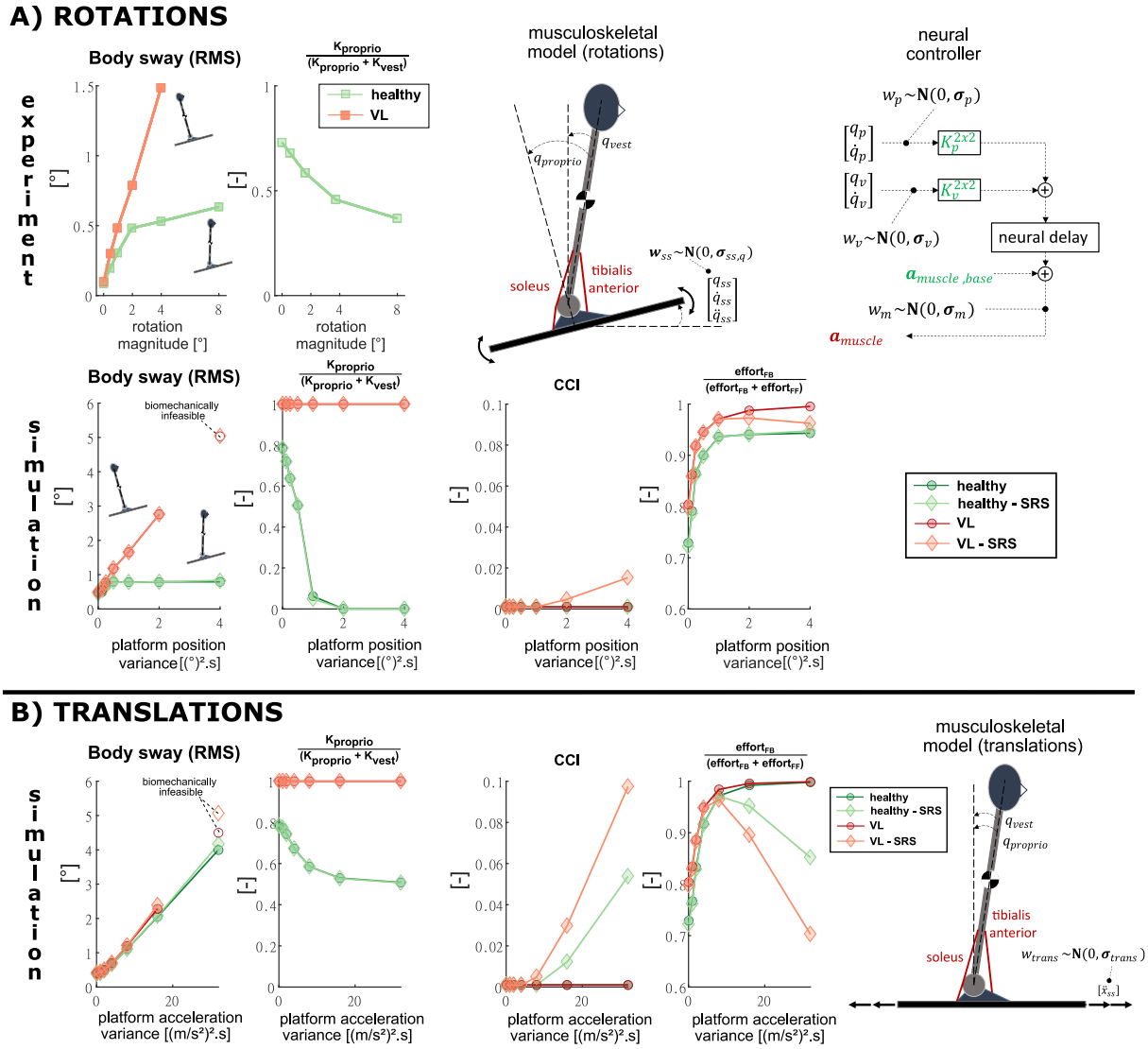

*Figure 1 – **A**: **ROTATIONS. Musculoskeletal and control model**. The proprioceptive (relative angle between the body and platform: $q_p, \dot{q}_p$) and vestibular (absolute body angle: $q_v, \dot{q}_v$) cues encode different information that is corrupted by proprioceptive and vestibular noise. The platform rotations are modeled by Gaussian noise of the platform position (q_{SS}), velocity ($\dot{q}_{SS}$) and acceleration ($\ddot{q}_{SS}$). a_{muscle} are muscle activations; $a_{muscle,base}$ are muscle baseline activations; K_p^{2x2} are proprioceptive feedback gains and K_v^{2x2} are vestibular feedback gains. **Experimental data and simulation results**. RMS body sway, relative proprioceptive feedback gains $\frac{\|K_{proprio}\|}{\|K_{proprio}\|+\|K_{vest}\|}$, co-contraction index (CCI) and contribution of expected effort from feedback to the total expected effort: $\frac{effort_{FB}}{effort_{FB}+effort_{FF}}$ for healthy and vestibular loss (VL) subjects with and without short-range-stiffness (SRS) modeled. **TRANSLATIONS. Musculoskeletal and control model**. The control model is identical to the model used to simulate the response to rotation perturbations, but in the case of translation perturbations the relative and absolute body angles are identical and vestibular and proprioceptive cues encode the same information. Platform translations are modeled by Gaussian noise of the linear platform acceleration ($\ddot{x}_{SS}$). **Simulation results**. The same outcome variables than for the rotation perturbations are shown.*

Stochastic optimal control of goal-directed reaching predicts experimental kinematics, movement variability and feedback modulation across different reaching tasks

In a second set of simulations, we demonstrate that stochastic optimal control using a nonlinear arm model can predict how nominal as well as perturbed reaching trajectories change as a function of task goals and environmental dynamics. We simulated the three point-to-point reaching tasks (Figure 2 – A) described in Nashed et al. [8]: reaching to a circular target (circle), reaching to a horizontal bar (bar),

and reaching to a circular target in the presence of a narrow obstacle (obstacle) (Figure 2 – A). Previously these reaching tasks were simulated using a point-mass model of the arm assuming OFC. To capture nonlinear inter-segment dynamics, we modeled the arm as a planar two-segment kinematic chain. To enable muscle activity predictions, the shoulder and elbow joints were each actuated by an agonist-antagonist pair of Hill-type muscles with rigid tendons. Net muscle excitations were a sum of time-varying feedforward excitations and delayed time-varying linear feedback of the end-effector (hand) kinematic error [8], [54]. Gaussian sensory noise and motor noise were added to the feedback signals and joint torques, respectively. The three different tasks were modeled by constraining the end-effector position variability to achieve the task requirements. Optimal feedforward controls, feedback gains and reference end-effector trajectories were computed by minimizing expected effort during unperturbed reaching, and the resulting optimal control policies were then used to generate stochastic forward simulations of both unperturbed and perturbed reaching.

In contrast to prior studies using a point mass model of the arm, our simulations predicted both unperturbed and perturbed reaching trajectories that were more similar to experimental findings [8]. All our optimal control policies met the required reaching end-point accuracy, for both perturbed and unperturbed reaching, as imposed for the different tasks in the stochastic optimal control problem formulations and in accordance with experimental data [8] (Figure 2 – B, end-point accuracy ellipses). In unperturbed reaches, kinematic trajectories were similar for our model, the point-mass model and the experimental data (Figure 2 – B, compare colored with black and grey trajectories). Like predictions based on the point-mass model, predictions based on our muscle-driven, multi-segment arm model were in line with the minimum intervention principle [3], [55] where kinematic deviations are only corrected when they interfere with the task goal: horizontal deviations are left uncorrected in the bar condition.

However, perturbed reach trajectories using our multi-segment, muscle-driven arm model were more similar to experimental trajectories, capturing asymmetry in perturbed reach trajectories [8] (Figure 2 – B, colored and black lines) that was not predicted based on point mass models (Figure 2 – B gray lines). In agreement with experiments, our model predicted corrections in the kinematic trajectory that occur late in the reaching movement for the ‘circle’ and ‘obstacle’ conditions (Figure 2 – B colored lines). Especially for the ‘bar’ condition our model predicted an overshoot of the hand in the vertical direction that was in strong agreement with experiments (Figure 2 – B perturbed trajectories, red and black lines). The vertical overshoot during perturbed reaching to a circular target predicted by our simulations was not present in the experimental data. In contrast, point-mass simulations predict earlier, symmetric, trajectory corrections without overshoot, likely due to the decoupled control of the vertical and horizontal degree of freedom. When reaching with a multi-segment arm, uni-directional perturbations cause multi-directional deviations in hand position and corrections in two dimensions need to be coordinated. Given the similarity in the underlying control hypothesis between our simulations and the point-mass simulations of Nashed et al. [8], this indicates the importance of accounting for nonlinear dynamics when predicting reaching movements [56], [57].

A novel aspect of our model is that muscle activations in response to perturbations could also be predicted and compared to available EMG recordings. Simulated corrective muscle activations were similar to recordings in the anterior deltoid and biceps, with larger corrections in the ‘circle’ than in the ‘bar’ condition (Figure 2 – C, blue vs red). Simulated corrective muscle activations in the ‘obstacle’ (Figure 2 – C, green) condition showed larger, rapid corrections that peaked earlier than in the circle and bar conditions. As EMG data was only available for the anterior deltoid and biceps in the circle and bar conditions, our simulated muscle activity of the antagonistic muscles and in the bar condition remains to be validated experimentally.

We found only limited co-contraction in our simulations that was similar across task conditions (Figure 2– D). As such, our simulations did not predict the small but significant increase in muscle co-contraction observed experimentally in the 'obstacle' compared to the 'circle' condition [8]. Note that we did not include short-range stiffness in our muscle model, which was necessary in the balance simulations to predict co-contraction, since short-range-stiffness contributions are negligible during movements over large ranges of motion [41].

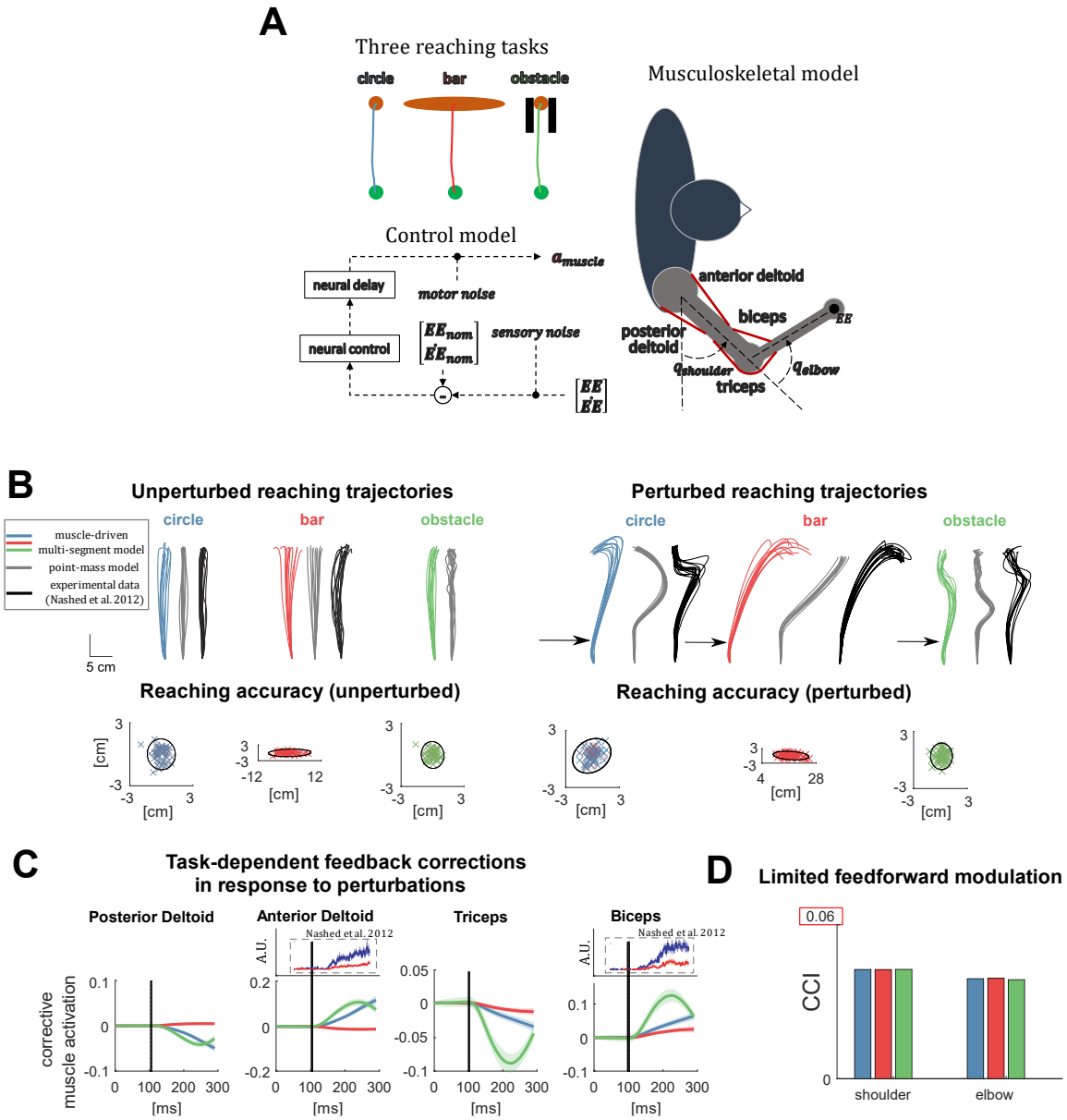

*Figure 2 – **A**: Schematic representation of the three reaching tasks and the musculoskeletal and control model. We simulated three different reaching tasks: (1) reaching towards a small circular target (blue), (2) reaching towards a horizontal bar (red), and (3) reaching towards a circular target in the presence of an obstacle (green). In all simulations, muscle excitations consist of feedforward and feedback contributions. The feedback controller is driven by the error between the end-effector kinematics ($\boldsymbol{EE}, \dot{\boldsymbol{EE}}$) and the nominal end-effector kinematics ($\boldsymbol{EE}_{ref}, \dot{\boldsymbol{EE}}_{ref}$) and is corrupted by sensory noise. Muscle forces are proportional to muscle activations $\boldsymbol{a}_{muscle}$, which are time-delayed muscle activations, and resulting joint torques are corrupted by motor noise. **B:** Unperturbed and perturbed reaching trajectories predicted by our model (colored), predicted with a point-mass model (grey) and measured (black). End-point accuracy simulated with our model for the three different reaching tasks. Ellipses denote 95% confidence regions. **C:** Simulated muscle-level corrective actions that result from optimal*

feedback in response to unexpected extension perturbations. For elbow and shoulder flexor muscles (anterior deltoid, biceps) we show experimental EMG data from Nashed et al. [8]. ***D:*** *Average simulated muscle co-contraction level for the shoulder and elbow joints for the three reaching tasks.*

Stiffness is modulated during goal-directed reaching in a divergent force field through changes in feedback but not feedforward control

To explore how the dynamics of the environment influences predicted contributions of muscle co-contraction and feedback control, we simulated reaching to a circular target in the presence of a divergent force field (Figure 3 – A). Although co-contraction has been observed during reaching in a force field, the relative contribution of muscle co-contraction and sensorimotor feedback control to increased endpoint stiffness [36], [56], [58], [59], is not known. We computed end-point stiffness as is done experimentally [60], i.e., by perturbing the hand in a specific direction in simulation and by dividing the resulting change in endpoint force by endpoint displacement over a short-time interval (150ms).

Similar to the experiments performed by Burdet et al. [35], [56] and Franklin et al. [36] our stochastic optimal control model predicted increased stiffness in the horizontal direction in the presence of a horizontal divergent force field of 200 N/m (Figure 3 – B). Our multi-segment muscle driven model predicted coupled changes in horizontal and vertical endpoint stiffness (Figure 3 – B) when reaching in an unstable force field, which would not be apparent from simple point-mass models as the vertical and horizontal degree of freedom are decoupled for such models.

In our model, the optimal strategy to increase stiffness in the presence of a divergent force field was to upregulate feedback control to all muscles without increasing co-contraction, while in experiments co-contraction increased significantly [36], [56], [58], [59] (Figure 3 – C and D). The small increase in simulated co-contraction around the elbow in the divergent force field (Figure 3 - D) likely resulted from small changes in the mean kinematic trajectory and hence feedforward excitations when the force field was applied.

Our simulations generated predictions on corrective muscle activity and perturbed reaching trajectories that remain to be validated in future experiments. The simulated corrective activity of all muscles in response to perturbations was higher when reaching in a divergent force field than in a stable environment (Figure 3 – C). Our simulations predict that perturbed reaching trajectories in the presence of a force field will not exhibit the overshoot in the vertical direction that was found in the absence of the force field.

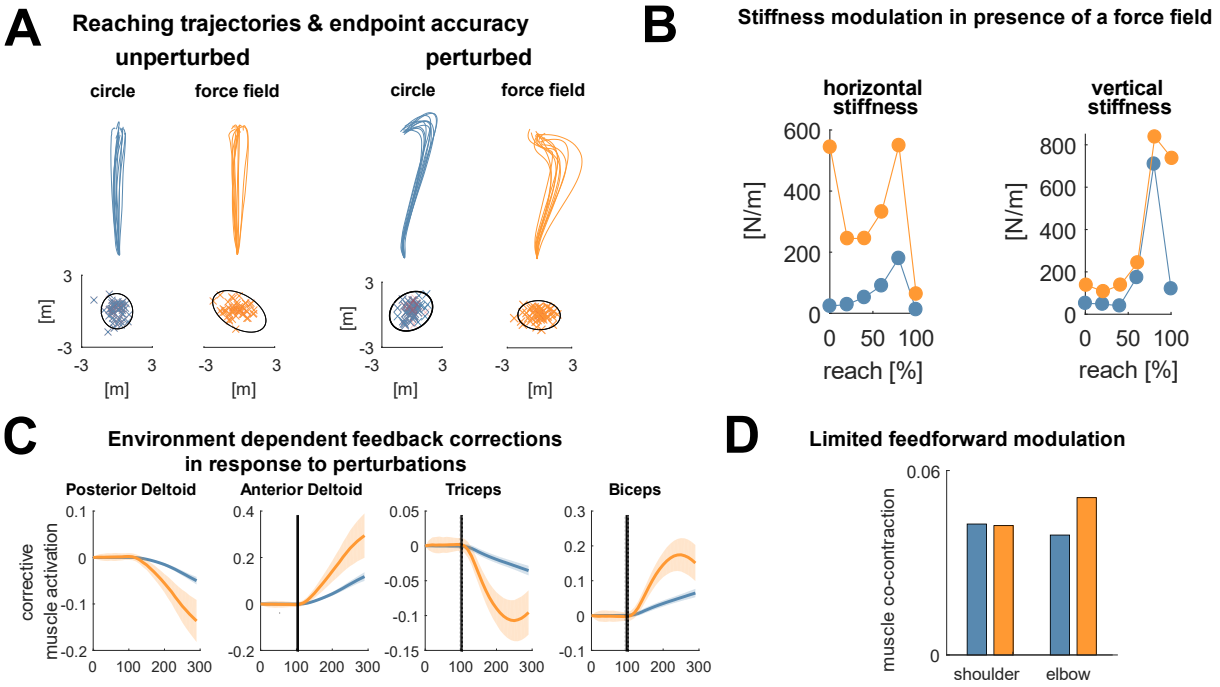

*Figure 3 – **A:** Unperturbed and perturbed reaching trajectories predicted in the presence ('force field') and absence ('circle') of a 200N/m divergent force field. Simulated end-point accuracy ellipses denote 95% confidence regions. **B**: Horizontal and vertical end-effector stiffness throughout the reaching movement for the optimal controllers in the absence and presence of the divergent force field. **C**: Simulated muscle-level corrective actions that result from optimal feedback in response to unexpected extension perturbations. **D:** Average muscle co-contraction level for the shoulder and elbow joint for the three reaching tasks.*

Discussion

Our major contribution was to apply a recently developed efficient approximate stochastic optimal control framework to simulations of motion enabling us to predict, for the first time, realistic movement trajectories and muscle coordination patterns emerging from nonlinear musculoskeletal dynamics, feedforward, and feedback neural control in the presence of noise. We used a generally applicable method to approximate the true stochastic optimal control problems by deterministic optimal control problems, which could be solved efficiently. The use of direct collocation and gradient-based optimization to solve the approximate deterministic problems facilitated the use of constraints, allowing us to distinguish effort optimization and task-level goals, such as accuracy, rather than to trade them of in the cost function. The framework allowed us to considerably extend the predictions of stochastic optimal control as a theory of motor coordination to the joint and muscle level, which enabled detailed comparison to experimental kinematic and EMG data. In particular, the addition of muscle models in stochastic optimal control simulations, demonstrated that muscle co-contraction can - in the presence of uncertainty in sensory information - minimize muscle effort required for a task. In balance control simulations, we demonstrated that benefits of increased impedance from muscle co-contraction depend on the intrinsic properties of the muscle and the interaction with delayed sensorimotor feedback mechanisms. Similarly, in reaching simulations, we demonstrated that multi-segment musculoskeletal dynamics are key to predicting complex perturbed and unperturbed reach trajectories under different task conditions, resulting from interactions between feedforward and feedback sensorimotor control mechanisms. Taken together, our results showed that complex features of motor control and movement

that were not captured by previous optimal control simulations can emerge from nonlinear stochastic optimal control processes. As such, our approximate stochastic optimal control framework provides a valuable tool to providing insight in neuromechanics of normal and possibly impaired movement that incorporates the complexities of the neuromusculoskeletal system and the effects of physiological noise.

Implementing a direct collocation approach to the solution of nonlinear stochastic optimal control problems increased computational efficiency and modelling flexibility, allowing neuro-musculoskeletal model complexity, and thereby fidelity, to be increased. Most prior methods have only allowed efficient solutions of linear, but not nonlinear, stochastic optimal control problems [6]–[8], [61], so that they were not capable of predicting many important variables causing movement. Stochastic optimal control simulations based on nonlinear dynamics have previously been performed using iterative Linear-Quadratic-Gaussian (iLQG) methods for reaching tasks [18]. However, such methods require a time-marching integration of the system dynamics under the current guess of the control law at each iteration to evaluate the nominal controls and state trajectories. Such shooting methods might be less suitable than collocation methods for movement tasks with less stable system dynamics, such as standing or walking. Besides, the LQG approach assumes a quadratic cost function and a linear and continuously time-varying feedback control law, which might not always represent the biological system. Finally LQG methods require achieving constraints on the mean state and state covariance (e.g. limiting the standard deviation of the end-point position of the hand in a reaching task) through penalty terms in the cost function, whose weights require tedious tuning. In contrast, our approach based on collocation and gradient-based optimization allows imposing such constraints in a direct and intuitive manner. A few previous studies [62], [63] have relied on direct collocation methods to solve stochastic optimal control problems but they evaluated the stochastic cost function and path constraints based on the simulation of a limited number of noisy episodes rather than describing the state distribution. For nonlinear systems with a limited number of degrees of freedom, such a sampling based approach appears tractable. However, with increasing degrees of freedom, the number of noisy episodes that is required to capture the underlying stochastic dynamics might become computationally intractable. Simulations based on too few episodes might result in problematic unstable and sub-optimal solutions. We overcame the limitations of prior methods by applying a recently proposed method to approximate stochastic optimal control problems by deterministic optimal control problems, developed for control engineering applications, to simulations of movement [26], [27]. The proposed approach is based on the assumption that the state distribution can be approximated by a Gaussian distribution and that the propagation of the state covariance can be described by the Lyapunov equation [28]. As such our framework allows optimal control problem formulations with any cost function design while feedback laws with any temporal and structural design are possible. Next, the possibility to impose path constraints on both the mean state and state covariance trajectories allows for an intuitive formulation of task requirements such as the desired accuracy.

Our novel framework allows task-goals to be specified as constraints allowing us to evaluate the minimal effort solution for a given task. It is still debated to what extent optimality assumptions capture human movement and what the optimality criteria underlying human movement are [11]. Previous stochastic optimal control simulations have typically been based on a multi-objective cost function reflecting a trade off in effort and accuracy [3], [7], [12], [17], [56], [64], [65]. In such simulations, the weights in the cost function must be tuned to produce simulations that match the desired accuracy. By using constraints to impose accuracy requirements and other task goals, task requirements can be separated from optimality principles that govern task execution within these requirements. We reproduced key features of movement kinematics and control by using expected effort as the sole performance criterion. Not only does the approximate stochastic optimal control framework remove the need of building multi-

objective cost functions, which might require considerable user intuition, minimizing effort within the solution space allowed by the task requirements might also be more representative of how humans approach a task. Rather than minimizing variability, humans might pick a control strategy that is 'good enough' [66]. For example, in standing a 'good enough' control strategy prevents a fall and for reaching a 'good enough' control strategy brings the hand in the target. The framework, based on direct collocation, can efficiently handle constraints offering flexibility in formulating the optimal control problem by for example imposing control bounds and constraining kinematic variability in agreement with task requirements. Our approach thus allowed us to further test effort minimization as the optimality criterion underlying human movement.

Our simulations suggest that muscle co-contraction might be a minimal effort strategy to achieve movement goals whereas it has often been seen as an energetically costly strategy to maximize accuracy. Here, we found that optimal contributions of muscle co-contraction varied as a function of the task, mechanical properties of the muscles, and sensory acuity. Our stochastic optimal control framework predicted co-contraction as a minimal effort strategy during perturbed standing balance, suggesting that a combination of co-contraction and feedback corrections is energetically more efficient than feedback corrections only. Prior models also predicted feedback modulation with changing sensory acuity, but did not include muscles that allowed for co-contraction as a complementary strategy [14], [42]. Conversely, the effect of muscle co-contraction on joint impedance has been shown with linearized muscle models, but did not consider contributions of feedback control [67]. Co-contraction reduces effort when task performance benefits from increased joint impedance and activation-dependent muscle properties allow to increase intrinsic mechanical impedance at reasonable costs. This seems to be the case in healthy subjects for translational but not rotational perturbations and in vestibular loss subjects for both translational and rotational perturbations but only when muscle short-range stiffness was taken into account.

Muscle co-contraction has been observed experimentally during reaching [68], especially in a divergent force field [56], [58], [59], but was not predicted by our stochastic optimal control simulations. This discrepancy might result from our framework not allowing predictions of the agonist-antagonist dual control strategy [60] enabled by muscle co-contraction. By co-contracting antagonistic muscles, it is possible to increase agonist activity and decrease antagonist activity simultaneously yielding a more efficient response to a perturbation. Although our approach to stochastic optimal control accounts for nonlinear state dynamics, it was still based on a linear approximation around the mean state trajectory to propagate the state covariance matrix. An important nonlinearity arises from muscle activity being bound between zero and one and hence, reductions in muscle activity are only possible when muscle activity is larger than zero. Yet this nonlinearity is not reflected in our approximation of the state covariance dynamics, which results in predicted reductions in muscle excitations if warranted for a perturbation, even when this would result in muscle excitations becoming smaller than zero. Hence, there is no need to increase baseline activity in our simulations to exploit the agonist-antagonist dual control strategy, which likely resulted in overly large predicted contributions of this strategy as they came at no cost. To further improve the realism of our simulations, we need to more accurately describe the nonlinearities in the dynamics of the state covariance. Other modelling assumptions might have influenced our estimates of muscle co-contraction to a smaller extent. On the one hand, we used an all or nothing approach to model short-range-stiffness whereas short-range-stiffness disappears when muscle stretch exceeds a certain threshold [41]. Therefore, short-range-stiffness might only contribute during low amplitude sway up to 3° [34], [41], and we might have overestimated its contribution when platform perturbations were high enough to induce large sway. On the other hand, we did not model that

co-contraction increases short-latency reflexes through gain scaling [69], [70], thereby underestimating the contribution of co-contraction to stabilizing reflexes during both standing and reaching.

A major contribution of our work was to create a framework for predicting how stochastic optimal control principles apply at the level of individual joints and muscles, which is difficult to impossible with currently available tools. Generating simulations that predict execution-level physiological variables that can be compared to experimental measures requires the subsystems, i.e. joints and muscles, from which those measures are obtained to be modeled. While it is known that using different levels of detail to represent the musculoskeletal dynamics lead to different simulated responses to perturbations if motor commands remained unchanged [71], optimal control predictions inform how the nervous system can exploit the nonlinear dynamics of the musculoskeletal system. As such the ability of stochastic optimal control to predict movement cannot be accurately validated using simple models. For example, our two-segment arm model yielded more realistic reach trajectories when reaching to different targets, especially in the presence of perturbations, when compared to prior predictions based on a point mass [8]. Similarly, simulations of endpoint stiffness in an unstable force field show, similar to experimental observations [36], [56], [58], [72], that the modulation of vertical stiffness is adapted together with horizontal stiffness because muscle activation affects both horizontal and vertical endpoint stiffness. These examples demonstrate how stochastic optimal control applied to muscle-driven models can be used to interpret complex motor coordination at the muscle level and to study control of redundant sets of muscles in the presence of noise.

Our novel computational framework leverages computational advances from deterministic movement simulations to enable predictions for stochastic movement simulations that may yield much insight into both normal and pathological movement control, as well as human-robot interactions. Under the assumption of stochastic optimal control, our movement predictions became more realistic when modelling neuro-musculoskeletal dynamics in more detail. Moving beyond deterministic simulations may enable coupled changes in complex, whole body movement and its neural control to be studied in both healthy and impaired movement. The interactions of feedforward and feedback neural control mechanisms with musculoskeletal mechanics is critical to consider in a highly redundant space of feasible neuromusculoskeletal solutions for movement, particularly in the presence of noise. Optimal control processes may also explain compensatory changes in neural control of movement in impaired motor control [73]. Moreover, the role of nonlinear musculoskeletal dynamics has been recently demonstrated to play a significant role in impaired motor control such as in spasticity [4]. Further, movement variability might complicate the control and design of exoskeletons and other assistive devices. Incorporating uncertainty and movement variability in simulations, that are often used to generate and test ideas before implementing these in reality, could facilitate the design process of assistive devices.

METHODS

Approximating the stochastic optimal control problem by a deterministic optimal control problem

We formulate simulations of movement in the presence of noise as stochastic optimal control problems. Due to the presence of noise, the system dynamics are stochastic: $\dot{x}(t) = f(x(t), u(t), w)$; with x the stochastic state trajectories, u the deterministic control trajectories and w a set of disturbances with a zero-mean Gaussian distribution (noise). To solve the stochastic optimal control problems, we approximate the stochastic state trajectories, which are in general non-normally distributed, by normally

distributed trajectories. As a result, we can describe the stochastic state trajectory by the mean state trajectory $x_{mean}(t)$ and state covariance trajectory $P(t)$. The dynamics of the mean state can be described by a deterministic approximation of the stochastic dynamics obtained by setting the disturbances to zero:

$$\dot{x}_{mean}(t) = f(x_{mean}(t), u(t), w = 0). \quad (1)$$

The dynamics of the state covariance can be described by the continuous Lyapunov differential equations based on a local first-order approximation of the nonlinear system dynamics around the mean state, corresponding to the propagation rules of an extended Kalman Filter ([30], [74]):

$$\dot{P}(t) = A(t)P(t) + P(t)A(t)^T + C(t)\Sigma_w' C(t)^T \quad (2)$$

$$A(t) = \left(\frac{\partial f}{\partial x}(t, x(t), u(t), w)\right)_{x(t)= x_{mean}(t)} \quad (3)$$

$$C(t) = \left(\frac{\partial f}{\partial w}(t, x(t), u(t), w)\right)_{x(t)= x_{mean}(t)} \quad (4)$$

Equations (1-4) form a deterministic approximation of the stochastic dynamics. Similarly, we can approximate the stochastic constraint functions $g(x(t))$ by a normal distribution with mean $\mu_{g(x)} = g(x_{mean})$, and standard deviation $\sigma_{g(x)} = \sqrt{\frac{\partial g}{\partial x} P(t) \frac{\partial g}{\partial x}^T}$. Using this approach, we can transform the stochastic optimal control problem into an approximate deterministic optimal control problem:

$$\min_{u(t)} \quad E[\int J\big(x_{mean}(t), u(t), P(t)\big)dt] \quad \text{expected cost (5)}$$

$$subject\ to \quad \dot{x}_{mean}(t) = f(x_{mean}(t), u(t), w = 0) \quad \text{mean state dynamics (6)}$$

$$\dot{P}(t) = A(t)P(t) + P(t)A(t)^T + C(t)\Sigma_w' C(t)^T \quad \text{covariance dynamics (7)}$$

$$g_i\big(x_{mean}(t), u(t)\big) + \gamma_i \sqrt{\frac{\partial g_i}{\partial x} P(t) \frac{\partial g_i}{\partial x}^T} \geq 0 \quad i = 1, \dots n_g \quad \text{path constraints (8)}$$

with γ_i a parameter determining the probability that the state trajectory fulfills the constraint and n_g the number of path constraints. Given the Gaussian approximation of the state distribution, γ_i would need to be infinitely large to impose the constraint over the whole distribution. In practice, we choose finite values for γ_i, where the chance of fulfilling the constraints is 95% when γ_i = 2, and 99.7% when γ_i = 3.

We solve the approximate deterministic optimal control problems using direct collocation with a trapezoidal integration scheme and mesh intervals of 10ms and solve the resulting large, but sparse nonlinear programming problems (NLP) with IPOPT [75]. We formulate all dynamics implicitly (details in the Supplementary Material) to improve the numerical condition of the NLP [4], [22], [76]. We use CasADi [77] to perform automatic differentiation, which improves the accuracy of the derivative computations and might reduce the number of operations through use of its reverse mode [19]. For details on the numerical implementation of the optimal control problems, we refer to the Supplementary Material.

Stochastic optimal control simulations of movement

We applied our stochastic optimal control framework to two fundamental movements that have been studied extensively: standing balance and goal-directed reaching. An overview of the musculoskeletal and motor control models is provided in Figure 1 and Figure 2. In general, we optimized both feedforward (i.e., open-loop) and feedback components (i.e. feedback gains) of the control law to

perform the prescribed movement task robustly with minimal expected effort. For standing balance, we imposed task robustness by requiring the solution to be asymptotically stable, i.e. the state covariance was constant. For reaching, we imposed the required accuracy of the reaching movement depending on the target shape.

Standing balance

We first give a general description of the optimal control problem, simulations and outcome measures. Dynamic equations and model parameters are described in more detail below.

General description of standing balance simulations and outcome measures

We modeled standing in the presence of platform perturbations based on an inverted pendulum (IP) model (mass: 70kg, length: 1m) linked to a rotatable and translational platform (Figure 1). Two antagonistic Hill-type muscles with rigid tendons actuated the ankle joint, i.e., the joint connecting the pendulum to the platform. The muscle properties (maximal isometric force F_{ISO}, tendon slack length l_T^s, optimal fiber length l_M^o, optimal pennation angle α, damping coefficient β; described in table 1) were taken from the soleus and tibialis anterior muscle of the OpenSim3.3 gait10dof18musc model [78]. Input to the Hill-type muscles were muscle activations, which were a sum of constant baseline activations ($a_{SOL,base}, a_{TA,base}$) and feedback activations ($a_{SOL,fb}, a_{TA,fb}$). Feedback excitations ($e_{SOL,fb}, e_{TA,fb}$) were a linear combination of the angle and angular velocity of the inverted pendulum with respect to the gravitational field, representing vestibular information, and of the angle and angular velocity of the inverted pendulum with respect to the platform, representing proprioceptive information. All feedback gains were constant in time. Feedback activations resulted from feedback excitations through first-order dynamics with a time constant (τ) of 150ms lumping together sensory and motor delays [79]. Gaussian vestibular ($w_{v,q}, w_{v,\dot{q}}$) and proprioceptive noise ($w_{p,q}, w_{p,\dot{q}}$) with respective variance $\sigma_{v,q}^2, \sigma_{v,\dot{q}}^2$ and $\sigma_{p,q}^2, \sigma_{p,\dot{q}}^2$ was added to both the vestibular and proprioceptive cues, additive motor noise (w_{SOL}, w_{TA}) with variance ($\sigma_{SOL}^2, \sigma_{TA}^2$) corrupted the muscle activations. All sensory and motor noise sources were independent.

To simulate random rotation perturbations, the platform angular position, velocity and acceleration were modeled as zero mean Gaussian noise ($w_{SS,q}, w_{SS,\dot{q}}, w_{SS,\ddot{q}}$) with constant variance ($\sigma_{SS,q}^2, \sigma_{SS,\dot{q}}^2, \sigma_{SS,\ddot{q}}^2$). We introduce the subscript 'ss' to indicate the variables related to the platform or support-surface and to avoid confusion with subscript 'p' for proprioception. To simulate random translation perturbations, we only needed to describe the platform translational acceleration as zero mean Gaussian noise ($w_{SS,trans}$) with variance ($\sigma_{SS,trans}^2$). We could ignore the random translational position and velocity of the platform as these affect neither the dynamics of the pendulum nor the proprioceptive and vestibular information (relative and absolute pendulum angles).

The task-goal during standing was to maintain a stable upright posture (asymptotic stability). Postural asymptotic stability, in the presence of noise, was modeled by constraining the mean angle of the pendulum to be upright with zero angular velocity, the mean state derivatives to be zero (mean pendulum position and velocity and muscle activations are constant in time), and the state covariance derivatives to be zero: $\dot{P} = 0$ (state covariance matrix was constant in time).

We solved for the muscle baseline activities and feedback gains given the described constraints while minimizing expected effort. Expected effort was modeled as the expected value of the sum of muscle excitations and muscle baseline activations squared:

$$E\left[\int [{a_{SOL,base}}^2 + {a_{TA,base}}^2 + e_{SOL,fb}(t)^2 + e_{SOL,fb}(t)^2]dt\right] \quad (9)$$

We performed simulations based on four different models. We performed simulations with the full feedback model, representing healthy subjects, and simulations with only proprioceptive feedback,

representing vestibular loss subjects. We performed these simulations based on two muscle models, a Hill-type muscle model described and a Hill-type model that was extended with short-range-stiffness (SRS). SRS was modeled by adding a spring with activation dependent stiffness in parallel to the contractile element producing a force

$$F_{SRS} = k_{SRS} \cdot F_{iso,max} \cdot a_{base} \cdot \left(\frac{\tilde{l}_m - \tilde{l}_{m,upright}}{\tilde{l}_{m,opt}} \right), \quad (10)$$

with a_{base} the muscle baseline activation, $\tilde{l}_m$ the muscle fiber length, $\tilde{l}_{m,upright}$ the muscle fiber length in upright position, $\tilde{l}_{m,opt}$ the optimal muscle fiber length and k_{SRS} the short-range-stiffness scaling factor, which was set to 1 [80]. We thus have four models: healthy ('healthy'), healthy with muscles including short-range-stiffness ('healthy - SRS'), vestibular loss ('VL'), vestibular loss with muscles including short-range-stiffness ('VL - SRS').

Our outcome measures were (1) body sway – described by the standard deviation of the normally distributed pendulum angle, (2) the relative contribution of proprioceptive feedback, $\frac{\|K_{proprio}\|}{\|K_{proprio}\|+\|K_{vest}\|}$, (3) the co-contraction index (CCI), given by baseline activity of the strongest muscle (soleus), and (4) the contribution of expected effort from feedback to the total expected effort: $\frac{effort_{FB}}{effort_{FB}+effort_{FF}}$.

Stochastic dynamics and model parameters

We indicated variables that are modeled as Gaussian noise in red. The state consisted of the ankle angle and angular velocity, $q_A, \dot{q}_A$ and the activation of soleus and tibialis anterior, a_{SOL} and a_{TA}:

$$\boldsymbol{x} = [q_A \quad \dot{q}_A \quad a_{SOL} \quad a_{TA}]. \quad (11)$$

The control law was parametrized by the baseline muscle activations, $\boldsymbol{a}_{base}$, and the constant feedback gains, $\boldsymbol{K}$:

$$\boldsymbol{a}_{base} = [a_{SOL,base} \quad a_{TA,base}]; \; \boldsymbol{K} = \begin{bmatrix} K_{q,prop}^{SOL} & K_{\dot{q},prop}^{SOL} & K_{q,vest}^{SOL} & K_{\dot{q},vest}^{SOL} \\ K_{q,prop}^{TA} & K_{\dot{q},prop}^{TA} & K_{q,vest}^{TA} & K_{\dot{q},vest}^{TA} \end{bmatrix}, \quad (12)$$

where SOL refers to the soleus and TA refers to the tibialis anterior. The dynamics were described by the equations of motion of the pendulum and the first order delay between excitation and activation. The equations of motion were expressed in a non-inertial reference frame by introducing fictitious forces due to the angular and translational platform acceleration:

$$\begin{bmatrix} \frac{dq_A}{dt} \\ \frac{d\dot{q}_A}{dt} \\ \frac{da_{SOL,fb}}{dt} \\ \frac{da_{TA,fb}}{dt} \end{bmatrix} = \begin{bmatrix} \dot{q}_A \\ \frac{mgl \cdot sin(q_A + w_{SS,q}) + T_{SOL+TA}}{ml^2+I} + \frac{ml \cdot sin(q_A)}{ml^2+I} w_{SS,trans} + w_{SS,\ddot{q}} \\ (e_{SOL,fb} - a_{SOL,fb})/\tau \\ (e_{TA,fb} - a_{TA,fb})/\tau \end{bmatrix}, \quad (13)$$

with m the pendulum mass, l the pendulum length, g the gravity constant, I the pendulum inertia, T_{SOL+TA} the torque generated by the soleus and tibialis anterior, and where feedback muscle excitations ($e_{SOL,fb}, e_{TA,fb}$) resulted from linear feedback of the feedback signal $\boldsymbol{y}_{fb}$:

$$\boldsymbol{y}_{fb} = \begin{bmatrix} q_A + w_{p,q} \\ \dot{q}_A + w_{p,\dot{q}} \\ q_A + w_{SS,q} + w_{v,q} \\ \dot{q}_A + w_{SS,\dot{q}} + w_{v,\dot{q}} \end{bmatrix}; \begin{bmatrix} e_{SOL,fb} \\ e_{TA,fb} \end{bmatrix} = \boldsymbol{K} \cdot \boldsymbol{y}_{fb} \quad (14)$$

Note that we assumed here that the platform's mean linear and angular position, velocity and acceleration were constant in time with constant variance. This differs from driving the platform with a zero-mean Gaussian input signal, which would lead to a monotonic increase of the variance in time. Instead, we implicitly assumed that a more clever platform controller was used.

The torque generated by the soleus and tibialis anterior muscles is a function of their forces and moment arms:

$$T_{SOL+TA} = F_{SOL} \cdot d_{SOL}(q_A) + F_{TA} \cdot d_{TA}(q_A). \quad (15)$$

with $d_{SOL}(q_A), d_{TA}(q_A)$ the soleus and tibialis anterior moment arms, which depend on the ankle angle q_A. Muscle forces depend on muscle activation and through the force-length-velocity properties of the muscle also on the muscle length (l_{SOL}, l_{TA}) and velocity ($\dot{l}_{SOL}, \dot{l}_{TA}$), which in turn are a function of the ankle angular position and velocity $q_A, \dot{q}_A$:

$$\begin{bmatrix} F_{SOL} \\ F_{TA} \end{bmatrix} = \begin{bmatrix} F_{ISO,SOL} \cdot [(a_{SOL,fb} + a_{SOL,base} + w_{SOL}) \cdot f_l(l_{SOL}) \cdot f_v(l_{SOL}, \dot{l}_{SOL}) + f_{p,SOL}(l_{SOL})] \\ F_{ISO,TA} \cdot [(a_{TA,fb} + a_{TA,base} + w_{TA}) \cdot f_l(l_{TA}) \cdot f_v(l_{TA}, \dot{l}_{TA}) + f_{p,TA}(l_{TA})] \end{bmatrix} \quad (16)$$

with f_l the active muscle force-length relationship, f_v the muscle force-velocity relationship, and f_p the passive muscle force-length relationship. The active force-length, force-velocity, and passive force-length relationships are described in [5].

Muscle-tendon lengths were approximated by the sum of a linear function, a sine, and a constant offset ($l_{MT} = a \cdot q + b \cdot \sin(c \cdot q) + d$) with a, b, c and d estimated by minimizing the least square error between this approximation and the muscle lengths obtained from the OpenSim gait10dof18musc model [81]. The moment-arms are computed as the derivatives of the muscle-lengths with respect to the angle: $d_{muscle} = \mathrm{a} + b \cdot c \cdot \cos(c \cdot q)$ [78].

Noise characteristics (summarized in Table 4) were based on preliminary simulations and experimental data [31]. Motor noise, added to muscle activations, had a standard deviation of 1% of the maximal signal based on force fluctuation measurements in different isometric tasks [82], [83], where a coefficient of variation between 1-5% was found. These measurements quantify motor noise indirectly as force-tracking errors might have other origins as well and we therefore selected the lower end of the measured variability to model motor noise. The relative values of proprioceptive and vestibular noise were selected such that the relative contribution of proprioceptive feedback, $\frac{\|K_{prop}\|}{\|K_{prop}\|+\|K_{vest}\|}$, was between 0.7-0.8 during optimal unperturbed standing in agreement with values identified from experiments by Peterka et al. [31]. The absolute values for sensory noise were selected such that during optimal unperturbed standing body sway, defined as the standard deviation of the pendulum angle, was ~0.3°, a typical value found in experiments of quiet standing in healthy subjects [84]. The values that determine the platform rotations, $\sigma^2_{SS,q}, \sigma^2_{SS,\dot{q}}, \sigma^2_{SS,\ddot{q}}$, were selected to mimic the rotational perturbations applied in [31]. In these experiments, the platform angular position, velocity and acceleration were not Gaussian. Here, we approximated the non-Gaussian experimental platform movements by zero-mean Gaussian platform movements with a standard deviation of half the amplitude of the experimental perturbations. The variance of the translational accelerations $\sigma^2_{SS,trans}$ were determined such that the healthy model for the maximal accelerations, under optimal control, reached a standard deviation of the ankle angle of 4°, a value that is typically not exceeded in continuous translation perturbation experiments [85], [86].

Table 1 - Muscle properties of model for perturbed standing simulations

Muscle properties soleus; tibialis anterior	
$F_{ISO}[N]$	5137; 3000
$l_T^s[m]$	0.2514;0.2228
$l_M^o[m]$	0.0528; 0.1028
α [rad]	0.4364; 0.0873
β	0.01; 0.01

Table 2 - Noise characteristics for perturbed standing balance simulations.

Sensory noise		**Motor noise**		$\sigma^2_{SS,\dot{q}}[(°/s)^2.s]$	0.001²; 0.3²; 0.6²; 1.2²; 2.4²; 4.8²; 9.6²
$\sigma^2_{p,q}[(°)^2.s]$	0.1²	$\sigma^2_{SOL}[(-)^2.s]$	0.01²	$\sigma^2_{SS,\ddot{q}}[(°/s^2)^2.s]$	0.001²; 1²; 2²; 2²; 2²; 2²; 2²
$\sigma^2_{p,\dot{q}}[(°/s)^2.s]$	0.2²	$\sigma^2_{TA}[(-)^2.s]$	0.01²	**Platform translations**	
$\sigma^2_{v,q}[(°)^2.s]$	0.3²	**Platform rotations**		$\sigma^2_{SS,trans}[(m/s^2)^2.s]$	0.001²; 0.0175²; 0.035²; 0.07²; 0.14²; 0.28²; 0.56²
$\sigma^2_{v,\dot{q}}[(°/s)^2.s]$	0.6²	$\sigma^2_{SS,q}[(°)^2.s]$	0.001²; 0.125²; 0.25²; 0.5²; 1²; 2²; 4²		

Note on the units of the noise variances. The time unit appears in the noise variance ([.s]) because we describe continuous-time Gaussian noise. If we perform a numerical integration and thus move to a discrete-time description of continuous noise the unit of time disappears by dividing the variance by the integration interval length (expressed in seconds). This makes sense if we reflect about a forward integration of a 1D point mass where the velocity has a continuous variance of e.g. 2 (m/s)².s. If we perform the numerical integration over an interval of 1s the discrete variance (Σ) is 2 (m/s)², we find that the variance of the position after 1s is equal to 2m²: $P_{k+1} = P_k + dt * \Sigma * dt' \rightarrow P_{k+1} = 0 + 1[s] * 2[(m/s)^2] * 1[s] = 2m^2$ *. If we perform the numerical integration over 1s using a time step of 0.1s the discrete variance is 20 (m/s)². We obtain* $P_{0.1s} = 0 + 0.1[s] * 20[(m/s)^2] * 0.1[s] = 0.2m^2$. *We obtain for* $P_{0.2s} = 0.2[m^2] + 0.1[s] * 20[(m/s)^2] * 0.1[s] = 0.4m^2$. *Finally,* $P_{1s} = 2m^2$.

Goal-directed reaching

General description of reach simulations and outcome measures

We modeled four reaching tasks based on a two-segment model, where the segments represent the upper and lower arm and are connected by hinge joints (Figure 2). An agonist-antagonist couple of Hill-type muscles with rigid tendons actuated each joint. The muscle properties (maximal isometric force F_{ISO}, tendon slack length l_T^s, optimal fiber length l_M^o, optimal pennation angle α, damping coefficient β; described in table 3) were based on the biceps brachialis, triceps, anterior deltoid and posterior deltoid of a full-body musculoskeletal OpenSim model [87], [88]. We adapted some muscle parameters to compensate for the absence of other (bi-articular) muscles by changing the relation between joint angles moment-arms and by adapting the force-length relation such that the muscles could generate force throughout the full range of the reaching movement. The muscles were stimulated by muscle excitations ($e_{ANTDEL}, e_{POSTDEL}, e_{BIC}, e_{TRI}$) that were a sum of feedforward and feedback excitations. Feedback excitations consisted of linear time-varying feedback of the end-effector (hand) position and velocity with respect to the nominal end-effector kinematics. The nominal end-effector kinematics was the end-effector kinematics due to the feedforward excitations in the absence of sensory and motor noise. Activations were related to excitations through first-order dynamics with a time constant (τ) of 150ms lumping together sensorimotor delays. Sensory noise was modeled by additive Gaussian noise on the

end-effector position (w_{EE_x}, w_{EE_y}) and velocity $(w_{\dot{E}E_x}, w_{\dot{E}E_y})$ with respective variance $(\sigma^2_{EE,x}, \sigma^2_{EE,y}, \sigma^2_{EE,\dot{x}}, \sigma^2_{EE,\dot{y}})$. The noisy end-effector positions and velocities were input to the feedback law. Motor noise was modeled by Gaussian motor noise added to each joint torque (w_s, w_e) with variance (σ_s^2, σ_e^2).

The task-goal was to perform a point-to-point reaching movement over a distance of 25cm in 0.5s with a pre-defined chance of the end effector ending up within the target, Reaching accuracy was imposed by limiting the variance of the horizontal and vertical end-effector position depending on the task requirements.

(1) Reaching towards a small circular target (circle) was modeled by constraining the standard deviation of the end-effector end-point horizontal and vertical positions to be smaller than 0.4cm.

(2) Reaching towards a horizontal bar (bar) was modeled by constraining the standard deviation of the end-effector end-point vertical position to be smaller than 0.4cm

(3) Reaching towards a circular target in presence of an obstacle was modeled by imposing the standard deviation of the end-effector end-point horizontal and vertical positions to be smaller than 0.4cm and the standard deviation of end-effector horizontal position during the second part (>0.25s) of the reaching trajectory to be smaller than 0.4cm

(4) Reaching towards a circular target in presence of a divergent force field of 200N/m was modeled by constraining the standard deviation of the end-effector end-point horizontal and vertical positions to be smaller than 0.4cm.

We solved for optimal control policies that minimized expected effort,

$$E\left[\int [e_{ANTDEL}(t)^2 + e_{POSTDEL}(t)^2 + e_{BIC}(t)^2 + e_{TRI}(t)^2]dt\right], \quad (17)$$

while fulfilling the task requirements for each of the specific tasks. We then used these optimal control policies to perform 100 forward simulations of unperturbed and perturbed reaching. The simulated extension perturbations matched the perturbations in the experiments described by Nashed et al. [8].

We computed the accuracy for the different optimal control policies in perturbed and unperturbed reaching by computing the 95% confidence ellipses of the end-point positions of the end-effector for the 100 simulations. We computed the corrective muscle activations for perturbed reaching by subtracting the mean muscle activations during unperturbed reaching from the muscle activations for each of the 100 perturbed reaching simulations. We computed the mean and standard deviation of these corrective muscle activations to analyze corrective behavior at the muscle level. We computed the co-contraction index throughout the reaching movement for each of the joints by averaging the joint-specific CCI over time. In this case, we computed the CCI as in [89]: $\frac{min\left(a_{flex}(t), a_{ext}(t)\right)}{\max\left(a_{flex}(t), a_{ext}(t)\right)} * (a_{flex}(t) + a_{ext}(t))$ where a_{flex} and a_{ext} are the activations of the flexor and extensor muscles at the joint.

Stochastic dynamics and model parameters

We indicated variables that are modeled as Gaussian noise in red. The state consisted of the ankle angle and angular velocity, $q_A, \dot{q}_A$ and the activation of soleus and tibialis anterior, a_{SOL} and a_{TA}:

We indicated variables that are described as constant zero-mean Gaussian noise in red. The state consisted of the joint angle angular positions (q_s, q_e) and velocities $(\dot{q}_s, \dot{q}_e)$, and the activations of the

anterior deltoid, the posterior deltoid, the biceps and the triceps muscles $(a_{ANTDEL}, a_{POSTDEL}, a_{BIC}, a_{TRI})$.

$$\boldsymbol{x} = [q_s \quad q_e \quad \dot{q}_s \quad \dot{q}_e \quad a_{ANTDEL} \quad a_{POSTDEL} \quad a_{BIC} \quad a_{TRI}]. \tag{18}$$

The control law was parametrized by the feedforward muscle excitation trajectories $\boldsymbol{e}_{ff}(t)$ and the time-varying feedback gains, $\boldsymbol{K}(t)$:

$$\boldsymbol{e}_{ff}(t) = \begin{bmatrix} e_{ff,ANTDEL}(t) \\ e_{ff,POSTDEL}(t) \\ e_{ff,BIC}(t) \\ e_{ff,TRI}(t) \end{bmatrix}; \; \boldsymbol{K}(t) = \begin{bmatrix} K_{q_s}^{ANTDEL}(t) & K_{q_e}^{ANTDEL}(t) & K_{\dot{q}_s}^{ANTDEL}(t) & K_{\dot{q}_e}^{ANTDEL}(t) \\ K_{q_s}^{POSTDEL}(t) & K_{q_e}^{POSTDEL}(t) & K_{\dot{q}_s}^{POSTDEL}(t) & K_{\dot{q}_e}^{POSTDEL}(t) \\ K_{q_s}^{BIC}(t) & K_{q_e}^{BIC}(t) & K_{\dot{q}_s}^{BIC}(t) & K_{\dot{q}_e}^{BIC}(t) \\ K_{q_s}^{TRI}(t) & K_{q_e}^{TRI}(t) & K_{\dot{q}_s}^{TRI}(t) & K_{\dot{q}_e}^{TRI}(t) \end{bmatrix} \tag{19}$$

The dynamics were described by the equations of motion and the first order delay between excitations and activations:

$$\begin{bmatrix} \frac{d\boldsymbol{q}}{dt} \\ \frac{d\dot{\boldsymbol{q}}}{dt} \\ \frac{d\boldsymbol{a}}{dt} \end{bmatrix} = \begin{bmatrix} \dot{\boldsymbol{q}} \\ M(\boldsymbol{q})^{-1}(C(\boldsymbol{q}, \dot{\boldsymbol{q}}) + \boldsymbol{T}_M + \boldsymbol{T}_{motor} + \begin{bmatrix} w_s \\ w_e \end{bmatrix}) \\ (\boldsymbol{e} - \boldsymbol{a})/\tau \end{bmatrix} \tag{20}$$

with $M(\boldsymbol{q})$ the mass-matrix of the arm model, $C(\boldsymbol{q}, \dot{\boldsymbol{q}})$ the term describing the Corriolis forces, $\boldsymbol{T}_M$ the shoulder and elbow joint torques generated by the muscles and $\boldsymbol{T}_{motor}$ the stochastic torque acting at shoulder and elbow resulting from motor noise w_s, w_e. The total muscle excitations were the result of feedforward and feedback control:

$$\boldsymbol{y}_{fb} = \begin{bmatrix} EE_x + w_{EE_x} \\ EE_y + w_{EE_y} \\ \dot{EE}_x + w_{\dot{EE}_x} \\ \dot{EE}_y + w_{\dot{EE}_y} \end{bmatrix} - EE_{ref}; \boldsymbol{e} = \boldsymbol{e}_{ff} + \boldsymbol{K} \cdot \boldsymbol{y}_{fb} \tag{21}$$

where the end effector positions (EE_x, EE_y) and velocities $(\dot{EE}_x, \dot{EE}_y)$ can be computed from the joint positions and velocities:

$$\begin{bmatrix} EE_x \\ EE_y \\ \dot{EE}_x \\ \dot{EE}_y \end{bmatrix} = f_{kin}(\boldsymbol{q}, \dot{\boldsymbol{q}}) \tag{22}$$

The reference end-effector trajectory is the end-effector trajectory in the absence of noise, which can thus be computed from the mean joint trajectories.

The shoulder and elbow torques generated by the different muscles depends on muscle forces and moment arms, which in turn depend on the shoulder and elbow joint angles:

$$T_M = \begin{bmatrix} F_{ANTDEL} \cdot d_{ANTDEL}(q_s) + F_{POSTDEL} \cdot d_{POSTDEL}(q_s) \\ F_{BIC} \cdot d_{BIC}(q_e) + F_{TRIC} \cdot d_{TRIC}(q_e) \end{bmatrix}; \tag{23}$$

with $d_{ANTDEL}(q_s), d_{POSTDEL}(q_s), d_{BIC}(q_e), d_{TRIC}(q_e)$ the muscle moment arms depending on the articulated joint angles. Muscle forces depend on muscle activation and through the force-length-velocity properties of the muscle also on the muscle length $(l_{ANTDEL}, l_{POSTDEL}, l_{BIC}, l_{TRIC})$ and velocity

$(\dot{l}_{ANTDEL}, \dot{l}_{POSTDEL}, \dot{l}_{BIC}, \dot{l}_{TRIC})$, which in turn were a function of skeleton positions and velocities $(q_s, q_e, \dot{q}_s, \dot{q}_e)$:

$$\begin{bmatrix} F_{ANTDEL} \\ F_{POSTDEL} \\ F_{BIC} \\ F_{TRIC} \end{bmatrix} = \begin{bmatrix} a_{ANTDEL} \cdot [F_{ISO,ANTDEL} \cdot f_l(l_{ANTDEL}) \cdot f_v(l_{ANTDEL}, \dot{l}_{ANTDEL}) + f_p(l_{ANTDEL})] \\ a_{POSTDEL} \cdot [F_{ISO,POSTDEL} \cdot f_l(l_{POSTDEL}) \cdot f_v(l_{POSTDEL}, \dot{l}_{POSTDEL}) + f_p(l_{POSTDEL})] \\ a_{BIC} \cdot [F_{ISO,BIC} \cdot f_l(l_{BIC}) \cdot f_v(l_{BIC}, \dot{l}_{BIC}) + f_p(l_{BIC})] \\ a_{TRIC} \cdot [F_{ISO,TRIC} \cdot f_l(l_{TRIC}) \cdot f_v(l_{TRIC}, \dot{l}_{TRIC}) + f_p(l_{TRIC})] \end{bmatrix} \quad (24)$$

with f_l the active muscle force-length relationship, f_v the muscle force-velocity relationship, and f_p the passive muscle force-length relationship. The active force-length, force-velocity, and passive force-length relationships are described in [5].

Muscle-tendon lengths were approximated by the sum of a linear function, a sine, and a constant offset ($l_{MT} = a \cdot q + b \cdot \sin(c \cdot q) + d$) with a, b, c and d estimated by minimizing the least square error between this approximation and the muscle lengths obtained from the upper-arm in a previously developed OpenSim model [88]. The moment-arms are computed as the derivatives of the muscle-lengths with respect to the angle: $d_{muscle} = \mathrm{a} + b \cdot c \cdot \cos(c \cdot q)$ [78].

We computed the variance of the end-effector position and velocity in the horizontal and vertical directions, used to define the constraints, based on the following equations:

$$Var(EE_x(t), EE_y(t), \dot{EE}_x(t), \dot{EE}_y(t)) = trace\left(\left(\frac{\partial f_{kin}(\boldsymbol{q}(t), \dot{\boldsymbol{q}}(t))}{\partial \boldsymbol{x}}\right) \boldsymbol{P}(t) \left(\frac{\partial f_{kin}(\boldsymbol{q}(t), \dot{\boldsymbol{q}}(t))}{\partial \boldsymbol{x}}\right)'\right) \quad (2526)$$

with $\boldsymbol{P}(t)$ the covariance matrix used to approximate the stochastic state.

Noise characteristics summarized in table 4 are based on preliminary simulations and experimental data. Similarly as in our standing balance simulations, we defined motor noise based on measures of force fluctuations to have a standard deviation of 1% of the maximal activation generated during a typical reaching movement [90]. The absolute values for sensory noise were selected such that during optimal unperturbed reaching to the circle target an end-point accuracy of 0.4cm was achievable but an accuracy of 0.2cm was not [8].

Table 3 - Musculoskeletal properties of model for goal-directed reaching

Skeletal properties upper arm; forearm		**Muscle properties** ANTDEL; POSTDEL; BIC; TRIC	
m [kg]	1.4;1.0	$F_{ISO}[N]$	1142.6; 259.88; 717.5; 525.1
l [m]	0.3; 0.33	$lT_s[m]$	0.093; 0.038; 0.098; 0.2
I[kg.m²]	0.0105; 0.0091	$lM_{opt}[m]$	0.0976; 0.1367; 0.1138; 0.1157
		α [rad]	0.3834; 0.3142; 0.1571; 0
		β	0.01; 0.01; 0.01; 0.01

Table 4 - Noise characteristics for goal-directed reaching simulations

Sensory noise		**Motor noise**	
$\sigma^2_{EE,x}[(mm)^2.s]$	0.6²	$\sigma^2_{SH}[(Nm)^2.s]$	0.1²
$\sigma^2_{EE,y}[(mm)^2.s]$	0.6²	$\sigma^2_{EL}[(Nm)^2.s]$	0.1²
$\sigma^2_{EE,\dot{x}}[(mm/s)^2.s]$	4.8²		
$\sigma^2_{EE,\dot{y}}[(mm/s)^2.s]$	4.8²		

References

[1] B. R. Umberger and R. H. Miller, "Optimal control modeling of human movement," *Handb. Hum. Motion*, vol. 1–3, pp. 327–348, 2018, doi: 10.1007/978-3-319-14418-4_177.

[2] C. L. Dembia, N. A. Bianco, A. Falisse, J. L. Hicks, and S. L. Delp, "OpenSim Moco: Musculoskeletal optimal control," doi: 10.1101/839381.

[3] E. Todorov and M. I. Jordan, "Optimal feedback control as a theory of motor coordination," 2002, doi: 10.1038/nn963.

[4] A. Falisse, G. Serrancolí, C. L. Dembia, J. Gillis, I. Jonkers, and F. De Groote, "Rapid predictive simulations with complex musculoskeletal models suggest that diverse healthy and pathological human gaits can emerge from similar control strategies," *J. R. Soc. Interface*, vol. 16, no. 157, Aug. 2019, doi: 10.1098/rsif.2019.0402.

[5] F. De Groote, A. L. Kinney, A. V. Rao, and B. J. Fregly, "Evaluation of Direct Collocation Optimal Control Problem Formulations for Solving the Muscle Redundancy Problem," *Ann. Biomed. Eng.*, vol. 44, no. 10, pp. 2922–2936, 2016, doi: 10.1007/s10439-016-1591-9.

[6] F. Crevecoeur and S. H. Scott, "Beyond Muscles Stiffness: Importance of State-Estimation to Account for Very Fast Motor Corrections," *PLoS Comput. Biol.*, vol. 10, no. 10, p. e1003869, Oct. 2014, doi: 10.1371/journal.pcbi.1003869.

[7] C. M. Harris, "On the optimal control of behavior: a stochastic perspective," *J. Neurosci. Methods*, vol. 83, pp. 73–88, 1998.

[8] J. Y. Nashed, F. Crevecoeur, and S. H. Scott, "Influence of the behavioral goal and environmental obstacles on rapid feedback responses," *J. Neurophysiol.*, vol. 108, no. 4, pp. 999–1009, Aug. 2012, doi: 10.1152/jn.01089.2011.

[9] F. Crevecoeur, S. H. Scott, and T. Cluff, "Robust Control in Human Reaching Movements: A Model-Free Strategy to Compensate for Unpredictable Disturbances," *J. Neurosci.*, vol. 39, no. 41, pp. 8135–8148, Oct. 2019, doi: 10.1523/JNEUROSCI.0770-19.2019.

[10] C. Harris and D. Wolpert, "Signal-dependent Noise determines Motor Planning," *Nature*, vol. 394, pp. 780–784, 1998, Accessed: Aug. 31, 2017. [Online]. Available: http://wexler.free.fr/library/files/harris (1998) signal-dependent noise determines motor planning.pdf.

[11] S. H. Scott, "The computational and neural basis of voluntary motor control and planning," *Trends in Cognitive Sciences*, vol. 16, no. 11. Elsevier, pp. 541–549, Nov. 01, 2012, doi: 10.1016/j.tics.2012.09.008.

[12] E. Todorov, "Optimality principles in sensorimotor control.," *Nat. Neurosci.*, vol. 7, no. 9, pp. 907–15, 2004, doi: 10.1038/nn1309.

[13] A. D. Kuo, "An optimal control model for analyzing human postural balance," *IEEE Trans. Biomed. Eng.*, vol. 42, no. 1, pp. 87–101, 1995, doi: 10.1109/10.362914.

[14] A. D. Kuo, "An optimal state estimation model of sensory integration in human postural balance," *J. Neural Eng*, vol. 2, pp. 235–249, 2005, doi: 10.1088/1741-2560/2/3/S07.

[15] J. Diedrichsen, "Optimal Task-Dependent Changes of Bimanual Feedback Control and Adaptation," *Curr. Biol.*, vol. 17, no. 19, pp. 1675–1679, Oct. 2007, doi: 10.1016/j.cub.2007.08.051.

[16] J. Diedrichsen, R. Shadmehr, and R. B. Ivry, "The coordination of movement: optimal

feedback control and beyond," *Trends in Cognitive Sciences*, vol. 14, no. 1. Elsevier Current Trends, pp. 31–39, Jan. 01, 2010, doi: 10.1016/j.tics.2009.11.004.

[17] H. Miyamoto, E. Nakano, D. M. Wolpert, and M. Kawato, "TOPS (Task Optimization in the Presence of Signal-Dependent Noise) Model," vol. 35, no. 11, pp. 48–58, 2004, doi: 10.1002/scj.10377.

[18] E. Todorov and W. Li, "A generalized iterative LQG method for locally-optimal feedback control of constrained nonlinear stochastic systems." Accessed: Sep. 09, 2020. [Online]. Available: www.cogsci.ucsd.edu/~todorov.

[19] A. Falisse, G. Serrancolí, C. L. Dembia, J. Gillis, and F. De Groote, "Algorithmic differentiation improves the computational efficiency of OpenSim-based trajectory optimization of human movement," *PLoS One*, vol. 14, no. 10, p. e0217730, Oct. 2019, doi: 10.1371/journal.pone.0217730.

[20] F. De Groote and A. Falisse, "Perspective on musculoskeletal modelling and predictive simulations of human movement to assess the neuromechanics of gait," *Proceedings. Biol. Sci.*, vol. 288, no. 1946, p. 20202432, Mar. 2021, doi: 10.1098/rspb.2020.2432.

[21] D. J. N. Limebeer and A. V Rao, "Faster, Higher and Greener. Vehicular Optimal Control.," *IEEE Control Syst. Mag.*, 2015, doi: 10.1109/MCS.2014.2384951.

[22] A. J. Van Den Bogert, D. Blana, and D. Heinrich, "Implicit methods for efficient musculoskeletal simulation and optimal control," in *Procedia IUTAM*, 2011, vol. 2, no. 2011, pp. 297–316, doi: 10.1016/j.piutam.2011.04.027.

[23] M. Ackermann and A. J. van den Bogert, "Optimality principles for model-based prediction of human gait," *J. Biomech.*, vol. 43, no. 6, pp. 1055–1060, 2010, doi: 10.1016/j.jbiomech.2009.12.012.

[24] C. F. Ong, T. Geijtenbeek, J. L. Hicks, and S. L. Delp, "Predicting gait adaptations due to ankle plantarflexor muscle weakness and contracture using physics-based musculoskeletal simulations," *PLoS Comput. Biol.*, vol. 15, no. 10, p. e1006993, Oct. 2019, doi: 10.1371/journal.pcbi.1006993.

[25] B. Houska and M. Diehl, "Robustness and Stability Optimization of Power Generating Kite Systems in a Periodic Pumping Mode," 2010, doi: 10.1109/CCA.2010.5611288.

[26] B. Houska and M. Diehl, "Robustness and stability optimization of power generating kite systems in a periodic pumping mode," in *Proceedings of the IEEE International Conference on Control Applications*, 2010, pp. 2172–2177, doi: 10.1109/CCA.2010.5611288.

[27] B. Houska, "Robust optimization of dynamic systems," 2011, Accessed: Sep. 04, 2020. [Online]. Available: http://dl.sanaye20.ir/RobustOptimazation.pdf.

[28] J. Gillis, "Practical methods for approximate robust periodic optimal control of nonlinear mechanical systems," no. March, 2015.

[29] J. Gillis and M. Diehl, "A positive definiteness preserving discretization method for lyapunov differential equations," in *Proceedings of the IEEE Conference on Decision and Control*, 2013, pp. 7759–7764, doi: 10.1109/CDC.2013.6761121.

[30] S. J. Julier, J. K. Uhlmann, and H. F. Durrant-Whyte, "New approach for filtering nonlinear systems," in *Proceedings of the American Control Conference*, 1995, vol. 3, pp. 1628–1632, doi: 10.1109/acc.1995.529783.

[31] R. J. Peterka, "Sensorimotor integration in human postural control," *J. Neurophysiol.*, vol. 88, no. 3, pp. 1097–1118, Sep. 2002, doi: 10.1152/jn.2002.88.3.1097.

[32] F. De Groote, J. L. Allen, and L. H. Ting, "Contribution of muscle short - range stiffness to

initial changes in joint kinetics and kinematics during perturbations to standing balance : A simulation study," *J. Biomech.*, vol. 55, no. 11, pp. 71–77, 2017, doi: 10.1016/j.jbiomech.2017.02.008.

[33] F. E. Zajac, "Muscle and tendon: properties, models, scaling, and application to biomechanics and motor control.," *Critical reviews in biomedical engineering*, vol. 17, no. 4. pp. 359–411, 1989.

[34] G. C. Joyce, P. M. H. Rack, and D. R. Westbury, "The mechanical properties of cat soleus muscle during controlled lengthening and shortening movements," *J. Physiol.*, vol. 204, no. 2, pp. 461–474, Oct. 1969, doi: 10.1113/jphysiol.1969.sp008924.

[35] E. Burdet, R. Osu, D. W. Franklin, T. E. Milner, and M. Kawato, "The central nervous system stabilizes unstable dynamics by learning optimal impedance," *Nature*, vol. 414, no. 6862, pp. 446–449, Nov. 2001, doi: 10.1038/35106566.

[36] D. W. Franklin, G. Liaw, T. E. Milner, R. Osu, E. Burdet, and M. Kawato, "Endpoint stiffness of the arm is directionally tuned to instability in the environment," *J. Neurosci.*, vol. 27, no. 29, pp. 7705–7716, Jul. 2007, doi: 10.1523/JNEUROSCI.0968-07.2007.

[37] A. Pedotti, V. V. Krishnan, and L. Stark, "Optimization of muscle-force sequencing in human locomotion," *Math. Biosci.*, vol. 38, no. 1–2, pp. 57–76, Jan. 1978, doi: 10.1016/0025-5564(78)90018-4.

[38] H. Van Der Kooij and R. J. Peterka, "Non-linear stimulus-response behavior of the human stance control system is predicted by optimization of a system with sensory and motor noise," *J. Comput. Neurosci.*, vol. 30, no. 3, pp. 759–778, 2011, doi: 10.1007/s10827-010-0291-y.

[39] F. B. Horak and A. D. Kuo, "Postural Adaptation for Altered Environments, Tasks, and Intentions," in *Biomechanics and Neural Control of Posture and Movement*, Springer New York, 2000, pp. 267–281.

[40] C. F. Runge, C. L. Shupert, F. B. Horak, and F. E. Zajac, "Ankle and hip postural strategies defined by joint torques," *Gait Posture*, vol. 10, pp. 161–170, 1999, doi: 10.1016/S0966-6362(99)00032-6.

[41] P. M. H. Rack and D. R. Westbury, "The short range stiffness of active mammalian muscle and its effect on mechanical properties," *J. Physiol.*, vol. 240, no. 2, pp. 331–350, Jul. 1974, doi: 10.1113/jphysiol.1974.sp010613.

[42] H. van der Kooij, R. Jacobs, B. Koopman, and F. van der Helm, "An adaptive model of sensory integration in a dynamic environment applied to human stance control," *Biol. Cybern.*, vol. 84, no. 2, pp. 103–115, Jan. 2001, doi: 10.1007/s004220000196.

[43] R. Fitzpatrick and D. I. McCloskey, "Proprioceptive, visual and vestibular thresholds for the perception of sway during standing in humans.," *J. Physiol.*, vol. 478, no. 1, pp. 173–186, Jul. 1994, doi: 10.1113/jphysiol.1994.sp020240.

[44] L. H. Ting and J. M. Macpherson, "Ratio of shear to load ground-reaction force may underlie the directional tuning of the automatic postural response to rotation and translation," *J. Neurophysiol.*, vol. 92, no. 2, pp. 808–823, Aug. 2004, doi: 10.1152/jn.00773.2003.

[45] L. Assländer and R. J. Peterka, "Sensory reweighting dynamics in human postural control," *J. Neurophysiol.*, vol. 111, no. 9, 2014, Accessed: Sep. 07, 2017. [Online]. Available: http://jn.physiology.org/content/111/9/1852.full.pdf+html.

[46] D. L. Sturnieks, R. S. George, and S. R. Lord, "Balance disorders in the elderly," *Neurophysiol. Clin. Neurophysiol.*, vol. 38, pp. 467–478, 2008, doi: 10.1016/j.neucli.2008.09.001.

[47] E. Kandel, J. Schwartz, T. Jessell, and S. Siegelbaum, "Principles of neural science," 2000,

Accessed: May 18, 2021. [Online]. Available: https://www.academia.edu/download/30536508/neuroscience_syllabus.pdf.

[48] S. H. Scott, "Optimal feedback control and the neural basis of volitional motor control," *Nat. Rev. Neurosci.*, vol. 5, no. 7, pp. 532–544, 2004, doi: 10.1038/nrn1427.

[49] J. M. Macpherson, D. G. Everaert, P. J. Stapley, and L. H. Ting, "Bilateral vestibular loss in cats leads to active destabilization of balance during pitch and roll rotations of the support surface," *J. Neurophysiol.*, vol. 97, no. 6, pp. 4357–4367, Jun. 2007, doi: 10.1152/jn.01338.2006.

[50] C. E. Craig, D. J. Goble, and M. Doumas, "Proprioceptive acuity predicts muscle co-contraction of the tibialis anterior and gastrocnemius medialis in older adults' dynamic postural control," *Neuroscience*, vol. 322, pp. 251–261, May 2016, doi: 10.1016/j.neuroscience.2016.02.036.

[51] L. M. Nashner, "Adapting reflexes controlling the human posture," *Exp. Brain Res.*, vol. 26, no. 1, pp. 59–72, Aug. 1976, doi: 10.1007/BF00235249.

[52] C. F. Runge, C. L. Shupert, F. B. Horak, and F. E. Zajac, "Role of vestibular information in initiation of rapid postural responses," *Exp. Brain Res.*, vol. 122, no. 4, pp. 403–412, 1998, doi: 10.1007/s002210050528.

[53] Y. Iwamoto, M. Takahashi, and K. Shinkoda, "Differences of muscle co-contraction of the ankle joint between young and elderly adults during dynamic postural control at different speeds," *J. Physiol. Anthropol.*, vol. 36, no. 1, pp. 1–9, Aug. 2017, doi: 10.1186/s40101-017-0149-3.

[54] F. Crevecoeur, S. H. Scott, and T. Cluff, "Behavioral/Cognitive Robust Control in Human Reaching Movements: A Model-Free Strategy to Compensate for Unpredictable Disturbances," 2019, doi: 10.1523/JNEUROSCI.0770-19.2019.

[55] N. Hogan, "Physical interaction via dynamic primitives," in *Springer Tracts in Advanced Robotics*, vol. 117, Springer Verlag, 2017, pp. 269–299.

[56] E. Burdet, D. W. Franklin, and T. E. Milner, *Human robotics : neuromechanics and motor control*. 2013.

[57] D. W. Franklin and D. M. Wolpert, "Computational mechanisms of sensorimotor control," *Neuron*, vol. 72, no. 3, pp. 425–442, 2011, doi: 10.1016/j.neuron.2011.10.006.

[58] D. W. Franklin, R. Osu, E. Burdet, M. Kawato, and T. E. Milner, "Adaptation to Stable and Unstable Dynamics Achieved by Combined Impedance Control and Inverse Dynamics Model," *J. Neurophysiol.*, vol. 90, no. 5, pp. 3270–3282, Nov. 2003, doi: 10.1152/jn.01112.2002.

[59] K. P. Tee, D. W. Franklin, M. Kawato, T. E. Milner, and E. Burdet, "Concurrent adaptation of force and impedance in the redundant muscle system," *Biol. Cybern.*, vol. 102, no. 1, pp. 31–44, Jan. 2010, doi: 10.1007/s00422-009-0348-z.

[60] E. Burdet, R. Osu, D. W. Franklin, T. Yoshioka, T. E. Milner, and M. Kawato, "A method for measuring endpoint stiffness during multi-joint arm movements," *J. Biomech.*, vol. 33, no. 12, pp. 1705–1709, Dec. 2000, doi: 10.1016/S0021-9290(00)00142-1.

[61] F. Crevecoeur, R. J. Sepulchre, J. L. Thonnard, and P. Lefèvre, "Improving the state estimation for optimal control of stochastic processes subject to multiplicative noise," *Automatica*, vol. 47, no. 3, pp. 591–596, Mar. 2011, doi: 10.1016/j.automatica.2011.01.026.

[62] A. D. Koelewijn and A. J. van den Bogert, "A solution method for predictive simulations in a stochastic environment," *J. Biomech.*, vol. 104, p. 109759, May 2020, doi: 10.1016/j.jbiomech.2020.109759.

[63] M. Afschrift, F. De Groote, S. Verschueren, and I. Jonkers, "Increased sensory noise and not muscle weakness explains changes in non-stepping postural responses following stance perturbations in healthy elderly," *Gait Posture*, 2017.

[64] T. Flash and N. Hogan, "The Coordination of Arm Movements: An Experimentally Confirmed Mathematical Model'," *J. Neurosci.*, vol. 5, no. 7, pp. 1688–1703, 1985, Accessed: Aug. 24, 2017. [Online]. Available: http://www.jneurosci.org/content/jneuro/5/7/1688.full.pdf.

[65] E. Todorov, "Communicated by Tamar Flash Stochastic Optimal Control and Estimation Methods Adapted to the Noise Characteristics of the Sensorimotor System," 2005. Accessed: Apr. 03, 2020. [Online]. Available: www.cogsci.ucsd.edu/.

[66] G. E. Loeb, "Optimal isn't good enough," *Biol. Cybern.*, vol. 106, no. 11–12, pp. 757–765, Dec. 2012, doi: 10.1007/S00422-012-0514-6.

[67] N. Hogan, "Adaptive Control of Mechanical Impedance by Coactivation of Antagonist Muscles," *IEEE Trans. Automat. Contr.*, vol. 29, no. 8, pp. 681–690, 1984, doi: 10.1109/TAC.1984.1103644.

[68] R. Osu *et al.*, "Optimal impedance control for task achievement in the presence of signal-dependent noise," *J. Neurophysiol.*, vol. 92, no. 2, pp. 1199–1215, Aug. 2004, doi: 10.1152/jn.00519.2003.

[69] J. A. Pruszynski, I. Kurtzer, and S. H. Scott, "The long-latency reflex is composed of at least two functionally independent processes," *J. Neurophysiol.*, vol. 106, no. 1, pp. 449–459, Jul. 2011, doi: 10.1152/jn.01052.2010.

[70] J. A. Pruszynski, I. Kurtzer, T. P. Lillicrap, and S. H. Scott, "Temporal Evolution of 'Automatic Gain-Scaling,'" *J. Neurophysiol.*, vol. 102, no. 2, pp. 992–1003, Aug. 2009, doi: 10.1152/jn.00085.2009.

[71] I. J. Pinter, A. J. Van Soest, M. F. Bobbert, and J. B. J. Smeets, "Conclusions on motor control depend on the type of model used to represent the periphery," *Biol. Cybern.*, vol. 106, no. 8–9, pp. 441–451, Oct. 2012, doi: 10.1007/s00422-012-0505-7.

[72] E. Burdet, R. Osu, D. Franklin, T. Milner, and M. Kawato, "The central nervous system stabilizes unstable dynamics by learning optimal impedance," *Lett. to Nat.*, vol. 414, no. 57, pp. 111–121, 2001, Accessed: Aug. 24, 2017. [Online]. Available: http://summerschool.stiff-project.org/uploads/tx_sibibtex/Burdet_Osu_Franklin_Milner_Kawato_-_The_central_nervous_system_stabilizes_unstable_dynamics_by_learning_optimal_impedance_-__Science_2001.pdf.

[73] D. B. Lockhart and L. H. Ting, "Optimal sensorimotor transformations for balance," *Nat. Neurosci. 2007 1010*, vol. 10, no. 10, pp. 1329–1336, Sep. 2007, doi: 10.1038/nn1986.

[74] R. E. Kalman, "A new approach to linear filtering and prediction problems," *J. Fluids Eng. Trans. ASME*, vol. 82, no. 1, pp. 35–45, Mar. 1960, doi: 10.1115/1.3662552.

[75] A. Wächter and L. T. Biegler, "On the implementation of an interior-point filter line-search algorithm for large-scale nonlinear programming," *Math. Program.*, vol. 106, no. 1, pp. 25–57, 2006, doi: 10.1007/s10107-004-0559-y.

[76] M. Millard, T. Uchida, A. Seth, and S. L. Delp, "Flexing Computational Muscle: Modeling and Simulation of Musculotendon Dynamics," *J. Biomech. Eng.*, vol. 135, no. 2, Feb. 2013, doi: 10.1115/1.4023390.

[77] J. A. E. Andersson, J. Gillis, G. Horn, J. B. Rawlings, and M. Diehl, "CasADi: a software framework for nonlinear optimization and optimal control," *Math. Program. Comput.*, vol. 11, no. 1, pp. 1–36, Mar. 2019, doi: 10.1007/s12532-018-0139-4.

[78] S. L. Delp *et al.*, "OpenSim: Open source to create and analyze dynamic simulations of movement," *IEEE Trans. Biomed. Eng.*, vol. 54, no. 11, pp. 1940–1950, 2007, doi: 10.1109/TBME.2007.901024.

[79] C. Le Mouel and R. Brette, "Mobility as the Purpose of Postural Control," *Front. Comput. Neurosci.*, vol. 11, p. 67, Jul. 2017, doi: 10.3389/fncom.2017.00067.

[80] F. De Groote, K. P. Blum, B. C. Horslen, and L. H. Ting, "Interaction between muscle tone, short-range stiffness and increased sensory feedback gains explains key kinematic features of the pendulum test in spastic cerebral palsy: A simulation study," *PLoS One*, vol. 13, no. 10, p. e0205763, Oct. 2018, doi: 10.1371/JOURNAL.PONE.0205763.

[81] A. Seth *et al.*, "OpenSim: Simulating musculoskeletal dynamics and neuromuscular control to study human and animal movement," *PLOS Comput. Biol.*, vol. 14, no. 7, p. e1006223, Jul. 2018, doi: 10.1371/journal.pcbi.1006223.

[82] K. E. Jones, A. F. Hamilton, and D. M. Wolpert, "Sources of Signal-Dependent Noise During Isometric Force Production," *J. Neurophysiol.*, pp. 1533–1544, 2002, doi: 10.1152/jn.00985.2001.

[83] N. B. Singh, N. König, A. Arampatzis, and W. R. Taylor, "Age-related modifications to the magnitude and periodicity of neuromuscular noise," *PLoS One*, vol. 8, no. 12, pp. 2–7, 2013, doi: 10.1371/journal.pone.0082791.

[84] J. M. Prado, T. A. Stoffregen, and M. Duarte, "Postural Sway during Dual Tasks in Young and Elderly Adults," *Gerontology*, vol. 53, no. 5, pp. 274–281, Aug. 2007, doi: 10.1159/000102938.

[85] A. D. Koelewijn and A. J. Ijspeert, "Exploring the Contribution of Proprioceptive Reflexes to Balance Control in Perturbed Standing," *Front. Bioeng. Biotechnol.*, vol. 8, p. 866, Aug. 2020, doi: 10.3389/fbioe.2020.00866.

[86] S. Sozzi, A. Nardone, and M. Schieppati, "Vision Does Not Necessarily Stabilize the Head in Space During Continuous Postural Perturbations," *Front. Neurol.*, vol. 10, no. JUL, p. 748, Jul. 2019, doi: 10.3389/fneur.2019.00748.

[87] H.-K. Kim and Y. Zhang, "Estimation of lumbar spinal loading and trunk muscle forces during asymmetric lifting tasks: application of whole-body musculoskeletal modelling in OpenSim," *http://dx.doi.org/10.1080/00140139.2016.1191679*, vol. 60, no. 4, pp. 563–576, Apr. 2016, doi: 10.1080/00140139.2016.1191679.

[88] A. van der Have, S. Van Rossom, and I. Jonkers, "Squat Lifting Imposes Higher Peak Joint and Muscle Loading Compared to Stoop Lifting," *Appl. Sci. 2019, Vol. 9, Page 3794*, vol. 9, no. 18, p. 3794, Sep. 2019, doi: 10.3390/APP9183794.

[89] K. S. Rudolph, M. J. Axe, and L. Snyder-Mackler, "Dynamic stability after ACL injury: Who can hop?," *Knee Surgery, Sport. Traumatol. Arthrosc.*, vol. 8, no. 5, pp. 262–269, Jul. 2000, doi: 10.1007/s001670000130.

[90] M. Russo, M. D'Andola, A. Portone, F. Lacquaniti, and A. d'Avella, "Dimensionality of joint torques and muscle patterns for reaching," *Front. Comput. Neurosci.*, vol. 8, no. MAR, p. 24, Mar. 2014, doi: 10.3389/fncom.2014.00024.